Identification of new therapeutic targets in *CRLF2*-overexpressing B-ALL through discovery of TF-gene regulatory interactions

Sana Badri[1,2,*], Beth Carella[1,3,*], Priscillia Lhoumaud[1], Dayanne M. Castro[2], Claudia Skok Gibbs[4], Ramya Raviram[1, 5], Sonali Narang[6], Nikki Evensen[6], Aaron Watters[4], William Carroll[6], Richard Bonneau[2,4,7,**], Jane A. Skok[1,**].

[1]Department of Pathology, New York University School of Medicine, New York, NY, USA.

[2]Department of Biology, Center for Genomics and Systems Biology, New York University, New York, NY, USA.

[3]Division of Blood and Marrow Transplantation and Cellular Therapies, UPMC Children's Hospital of Pittsburgh, Pittsburgh, PA.

[4]Flatiron Institute, Center for Computational Biology, Simons Foundation, New York, NY, USA.

[5]Department of Chemistry and Biochemistry, University of California, San Diego, CA, USA.

[6]Perlmutter Cancer Center, Departments of Pediatrics and Pathology, New York, NY, USA.

[7]Department of Computer Science, Courant Institute of Mathematical Sciences, New York, USA.

[*] These authors contributed equally to this manuscript

[**] Correspondence and requests for materials should be addressed to:

e-mail: rb133@nyu.edu (Richard Bonneau) jane.skok@med.nyu.edu (Jane A. Skok)

ABSTRACT

Although genetic alterations are initial drivers of disease, aberrantly activated transcriptional regulatory programs are often responsible for the maintenance and progression of cancer. *CRLF2*-overexpression in B-ALL patients leads to activation of JAK-STAT, PI3K and ERK/MAPK signaling pathways and is associated with poor outcome. Although inhibitors of these pathways are available, there remains the issue of treatment-associated toxicities, thus it is important to identify new therapeutic targets. Using a network inference approach, we reconstructed a B-ALL specific transcriptional regulatory network to evaluate the impact of *CRLF2*-overexpression on downstream regulatory interactions.

Comparing RNA-seq from *CRLF2*-High and other B-ALL patients (*CRLF2*-Low), we defined a *CRLF2*-High gene signature. Patient-specific chromatin accessibility was interrogated to identify altered putative regulatory elements that could be linked to transcriptional changes. To delineate these regulatory interactions, a B-ALL cancer-specific regulatory network was inferred using 868 B-ALL patient samples from the NCI TARGET database coupled with priors generated from ATAC-seq peak TF-motif analysis. CRISPRi, siRNA knockdown and ChIP-seq of nine TFs involved in the inferred network were analyzed to validate predicted TF-gene regulatory interactions.

In this study, a B-ALL specific regulatory network was constructed using ATAC-seq derived priors. Inferred interactions were used to identify differential patient-specific transcription factor activities predicted to control *CRLF2*-High deregulated genes, thereby enabling identification of new potential therapeutic targets.

Keywords: Transcriptional Regulatory Network, B-ALL, CRLF2, Leukemia, Transcription Factor Activity, TARGET, ATAC-seq, Network Inference

49 **INTRODUCTION:**

50 Acute lymphoblastic leukemia (ALL) is the most common cancer in children. Historically,
51 clinical criteria have driven risk stratification for these patients, however over time many genetic
52 alterations have been identified as prognostic predictors. Several groups have described varied
53 genetic signatures associated with pediatric ALL with the aim of elucidating their contributions to
54 leukemogenesis[1,2]. Improved risk stratification based on genetic signature has altered treatment
55 and led to significant improvements in overall survival[3]. However, about 20% of patients fail
56 current treatment strategies or die following relapse. Moreover, adults with ALL have a worse
57 prognosis and an average overall survival of 35-50%[3]. Therefore, it is important to gain a better
58 understanding of the mechanisms by which genetic alterations drive leukemogenesis to refine
59 therapies that target the disease-essential pathways involved[4].

60 Genetic alterations that lead to overexpression of the cytokine receptor-like factor 2
61 (*CRLF2*) gene have been associated with a high-risk subset of pediatric patients with B-cell
62 acute lymphoblastic leukemia (B-ALL). The *CRLF2* gene encodes the thymic stromal
63 lymphopoietin receptor (TSLPR) which forms a heterodimer with IL-7 receptor alpha (IL7RA) to
64 bind TSLP[5]. Binding of TSLP to the IL7RA-TSLPR complex signals the phosphorylation of
65 Janus kinase 1 (JAK1) and Janus kinase 2 (JAK2), leading to the activation of the JAK-STAT
66 signaling pathway[6]. Studies have shown that stimulation of TSLP in B-ALL not only induces
67 activation of the JAK-STAT pathway, but also activates the PI3K/mTOR[7] and ERK/MAPK
68 signaling pathways[3].

69 *CRLF2* overexpression occurs in 5-15% of patients with B-ALL and in 50-60% of
70 pediatric B-ALL patients with Down syndrome (DS)[6,8]. Overexpression can occur either from a
71 chromosomal translocation between *CRLF2* and the immunoglobulin heavy chain locus (*IGH*)
72 on chromosome 14 (*IGH-CRLF2*) or from an interstitial deletion of the pseudoautosomal region
73 of the X/Y chromosomes resulting in the fusion of *CRLF2* to the *P2RY8* gene (*P2RY8-CRLF2*)[9]
74 as shown in **Figure 1a**. *CRLF2* deregulation very rarely occurs via activating mutations of

75 *CRLF2*. *IGH-CRLF2* translocation occurs in precursor cells and is thought to result from
76 aberrant rejoining during V(D)J-recombination[10,11]. This translocation is most commonly found in
77 adolescents and adult patients and is typically associated with a poor prognoses, while the
78 *P2RY8-CRLF2* fusion is found in younger patients[3].

79 *CRLF2* chromosomal alterations are often accompanied by mutations in *JAK1*, *JAK2*
80 and *Ikaros* (*IKZF1*) genes. Several groups have suggested that aberrant *CRLF2* signaling
81 cooperates with mutant JAK and IKZF1 activity to promote the development of leukemia[9,12,13].
82 As a result, the focus has shifted towards the use of signal transduction inhibitors (STIs) to
83 target JAK-STAT, PI3K and MAPK signaling pathways[3]. Although, STIs have shown promise in
84 early clinical trials[14-16], broad application of signal transduction inhibitors is challenging due to
85 the interconnected roles of their targets in biological processes (i.e. JAK kinases) including
86 immunity and hematopoiesis[17]. Moreover, it has been shown that mutated *JAK2* is required for
87 the initiation of leukemia, but it is not necessary for its maintenance [18].

88 More recently, studies have constructed short and long chimeric antigen receptor (CAR)-
89 expressing T-cells to target *CRLF2* receptor and have demonstrated only the short CARs
90 targeting *CRLF2* can eliminate the leukemia in cell lines and xenograft models of *CRLF2*-
91 overexpressing ALL[19]. *CRLF2*-targeted CAR T cells represent a powerful immunotherapeutic
92 strategy for this cohort of B-ALL patients, nonetheless there are severe toxicity issues
93 associated with this type of therapy, related to damage of normal tissues that express this
94 antigen[20].

95 Exome and targeted sequencing of DS-ALL with *CRLF2* rearrangements has uncovered
96 driver mutations in *KRAS* and *NRAS* that are mutually exclusive to *JAK* mutations. *RAS* and
97 *JAK* mutations appear to occur at a similar frequency. Analysis of clonal architecture
98 demonstrates that the majority of clones initiated by *CRLF2* rearrangements are expanded into
99 distinct sub-clones by both *RAS* and *JAK2* mutations. Interestingly, the majority of relapsed
100 cases switch from a *JAK2*-mutated sub-clone to a *RAS*-mutated sub-clone, indicating there are

101 alternate drivers in relapsed *CRLF2*-overexpressing DS-ALL[21]. Although, this particular study
102 focused on DS-ALL, there is evidence that alternate genes can be responsible for the
103 maintenance of *CRLF2*-overexpressing cells[18], therefore, there is a need to more closely
104 investigate the impact of the altered *CRLF2* in B-ALL downstream of oncogenic signaling, to
105 identify alternate targets that can be evaluated for therapy.

106 To address the issue of alternate targets, we first sought to identify transcriptional
107 regulators that control differentially expressed genes associated with *CRLF2*-overexpression
108 through a comparative analysis of *CRLF2*-High cells versus other B-ALL samples that express
109 *CRLF2* at low levels in primary patient samples. Differential analysis of RNA-seq samples
110 resulted in robust genome-wide gene expression changes, with an expected significant
111 enrichment in cytokine-mediated signaling pathways. Using ATAC-seq data, patient-specific
112 chromatin accessibility landscapes were defined and interrogated to identify altered regions that
113 could be linked to transcriptional changes. While strong changes in accessibility were detected
114 in patients, only a proportion of these were linked to transcriptional changes. As a result, we
115 hypothesized that differential binding of TFs at ATAC-seq peaks are influencing gene
116 expression changes.

117 Using 868 B-ALL patient samples from the NCI TARGET database, we constructed A B-
118 ALL transcriptional network to define the interactions between transcription factors (TFs) and
119 the genes they regulate[22-24]. With RNA-seq, ATAC-seq, and TF-motif analysis, we inferred the
120 targets of TFs linked to the gene set associated with the *CRLF2*-High cohort using the
121 Inferelator algorithm[25,26]. The network was then used to predict differential transcription factor
122 activity (TFA) in *CRLF2*-High versus other B-ALL (*CRLF2*-Low) patient samples. This approach
123 enabled the identification of a *CRLF2*-High associated sub-network consisting of thirty-four
124 potential regulators of differentially expressed genes (including FOXM1, ETS2, FOXO1).
125 Several of the differential gene targets of these TFs (i.e. *PIK3CD*, *TNFRSF13C, PTPN7, GAB1*
126 and *TCF4)* are conserved in CRLF2 High versus Low patient-derived cell lines and have been

127 previously implicated in leukemias. The network-based approach we applied has been similarly
128 implemented in several other systems to infer regulatory interactions that have been
129 experimentally validated[27-30]. To validate TF-gene inferred interactions, we analyzed CRISPRi,
130 siRNA knockdown, and ChIP-seq ENCODE datasets in K562 and GM12878 cells involving 9
131 individual TFs. This resulted in the validation of gene targets for each TF further supporting the
132 network-based approach applied in this study. Thus, we uncovered a number of genes along
133 with their regulators that could contribute to the maintenance of leukemia and which act as
134 potential candidates for therapeutic targeting in *CRLF2*-High B-ALL.
135

136 **RESULTS**

137 **Genome-wide transcriptional changes in *CRLF2*-overexpressing primary patient samples**

138 Traditional chemotherapy is non-specific and targets rapidly dividing cells. Thus, toxicity
139 results in injury to healthy cells, causing further morbidity[31]. To reduce overall toxicity and
140 improve prognosis, most research has been directed towards understanding the underlying
141 molecular pathology of the leukemia. In this study, we focused on identifying regulatory
142 interactions associated with overexpression of *CRLF2* with the goal of finding new potential
143 therapeutic targets in this subset of B-ALL patients.

144 Gene expression profiles associated with *CRLF2* overexpression were identified by
145 comparing RNA-sequencing from 15 CRLF2-overexpressing patients (CRLF2-High) and 15
146 patients with low levels of *CRLF2* (Other B-ALL). Principal component analysis was performed
147 on gene expression levels across all 30 primary patient samples. This revealed a clear
148 separation between the two groups of patients (**Fig 1b**). Principal component analysis with
149 samples labeled according to batch do not demonstrate a batch effect (**Supplementary Fig.**
150 **1a**).

151 To further analyze the changes in gene expression between *CRLF2*-High and other B-
152 ALL patient samples we performed differential expression analysis using DESeq2[32]. This

153 analysis uncovered a total of 3,586 de-regulated genes with an adjusted p-value of less than
154 0.01 and |log_2FoldChange| >2 (**Fig. 1c, Supplemental Table 1**). Of these 1470 genes (~41%)
155 were up-regulated and 2116 (~59%) down-regulated in the *CRLF2*-High patients. In addition,
156 hierarchical clustering of the 3,586 differentially expressed genes shown in the **Figure 1d**
157 heatmap highlights the prominent transcriptional changes associated with overexpression of
158 *CRLF2*.

159 *CRLF2*-High patient samples clearly exhibit up-regulation of *CRLF2* (log_2FoldChange=
160 10.12) compared to control B-ALL patient samples as shown by RNA-seq tracks on IGV
161 (**Supplementary Fig. 1b**). Based on previous findings we expected to find evidence for
162 activation of JAK-STAT signaling. Indeed, in *CRLF2*-High samples *SOCS2*, a downstream
163 target of JAK/STAT signaling which encodes a SOCS protein that inhibits cytokine signaling as
164 part of a classical feedback loop[33], was statistically significantly up-regulated (log_2FoldChange=
165 4.30) (**Supplemental Table 1**). Thus, consistent with previous findings[34], JAK-STAT[3,4] signaling
166 appears to be activated in these samples.

167 GSEA was applied on the normalized expression counts of the 3,586 differentially
168 expressed genes using the molecular signatures (MSigDB) database to identify enriched
169 hallmark gene sets that represent well-defined biological processes. Significant pathways with
170 p-value<0.01 and FDR=1% (**Supplemental Table 2**) were enriched including IL2-STAT5 and
171 cytokine mediated signaling (**Supplemental Fig. 1c-1h**).

172

173 ***CRLF2*-overexpression leads to promoter-enriched ATAC-seq changes in patient**
174 **samples.**

175 To further investigate the impact of *CRLF2* overexpression, we asked whether CRLF2-
176 High associated transcriptional changes were accompanied by changes in chromatin
177 accessibility. For this we analyzed ATAC-sequencing and compared chromatin accessibility in
178 *CRLF2*-High versus other B-ALL patient samples (7 *CRLF2*-High and 6 other B-ALL). PCA

179 analysis on normalized ATAC-seq signal clearly separated the two conditions (**Figure 2a**).
180 Differential analysis of all the ATAC-seq peaks identified 700 regions that were more accessible
181 and 978 regions with reduced accessibility in the *CRLF2*-High versus low (**Fig. 2b-c**).
182 A total number of 115,457 ATAC-seq peaks across all patients were assigned to
183 promoters (within 3kb of TSS), UTRs, exons and introns of genes (**Fig. 2d**). Significant
184 differential ATAC-seq peaks (n=1,678) were similarly annotated (**Fig. 2e**) and more highly
185 enriched (~47%) at promoter regions compared to all peaks (~29%). There were 317 (18.9%)
186 differential ATAC-seq peaks associated with significant differentially expressed genes (n=268),
187 either on promoters or gene bodies. The majority of the differential ATAC-seq peaks (223) that
188 overlap differentially expressed genes were concordantly regulated, with the exception of 94
189 ATAC-gene pairs. Discordant ATAC-gene pairs could be representative of silencers and their
190 gene targets. For example, a decrease in accessibility can impair binding of a silencer to its
191 gene target and therefore lead to an increase in that gene's expression (**Fig. 2f**). Furthermore,
192 about 79% (177/223) of concordant pairs represented ATAC-seq peaks with decreasing
193 accessibility associated with genes exhibiting reduced expression. An example of this is shown
194 in **Figure 2g**, where an ATAC-seq peak with significantly decreased accessibility is associated
195 with down-regulation of receptor tyrosine kinase *KIT* in *CRLF2*-High patients. Importantly, the
196 majority of transcriptional changes were not associated with significant changes in chromatin
197 accessibility near the promoter or within the gene bodies (3328/3596 genes). In sum,
198 overexpression of *CRLF2* leads to genome-wide chromatin accessibility changes enriched at
199 promoter regions with a small proportion linked to significant transcriptional changes.
200

201 **Construction of a B-ALL regulatory network using ATAC-motif derived priors**

202 *CRLF2* overexpression activates a signaling cascade that involves many TF regulators
203 and gene targets. To examine these connections, we wanted to first identify which TFs could
204 potentially be regulating the differentially expressed genes in *CRLF2*-High versus other B-ALL
205 patient cohorts, and second to infer the relationship between these TFs and their target genes.
206 To address this, we performed TF-motif analysis, using Analysis of Motif Enrichment (AME)[35] to
207 identify enriched TF motifs at promoter-annotated differentially accessible ATAC-seq peaks
208 compared to shuffled input control sequences. Using an adjusted fisher p-value<1^{e-13}, 138
209 enriched TF motifs were defined at differentially accessible promoter peaks that could be
210 important for the *CRLF2*-High associated gene signature (**Supplemental Fig. 3a**).

211 To better understand the relationship between candidate TF regulators identified in
212 **Supplemental Fig. 3a** and the genes they potentially regulate, we sought to infer a
213 transcriptional regulatory network using the Inferelator algorithm[25,26]. The main limitation of
214 network inference is the sample size (the limited number of samples with an *CRLF2*-High
215 rearrangement). To model transcriptional interactions in a B-ALL specific context requires a
216 large dataset that includes hundreds of B-ALL patient samples, not limited to samples with a
217 specific genetic alteration. For this we made use of the TARGET initiative and analyzed 868 B-
218 ALL RNA-seq samples that were used to obtain a normalized gene expression matrix that could
219 be used for the construction of a B-ALL specific regulatory network.

220 There are three major steps involved in inferring a transcriptional regulatory network,
221 including generating priors, estimating transcription factor activities, and modeling gene
222 expression with regularized regression. To generate priors, recent studies have incorporated
223 prior information from different data types, like ChIP-seq, ATAC-seq, and TF-motif analysis to
224 associate TFs to their putative gene targets and this has considerably improved network
225 inference [27-29,36]. Thus, we focused on combining chromatin accessibility data from the *CRLF2*-

226 High and Low patients with TF-motif analysis to generate priors and acquire the TF-gene
227 associations. First, all ATAC-seq peaks found within a 20kb window upstream of a gene's
228 transcription start site (TSS) were assigned to that gene. Second, FIMO was used to analyze all
229 known TF motifs enriched within gene-associated ATAC-seq peaks. Lastly, TF motifs were
230 aggregated across all ATAC-seq peaks for each gene. For each TF motif-gene association, a
231 score, a p-value and an adjusted p-value was computed. Only TF-gene associations that had an
232 adjusted p-value less than 0.01 were retained (**Fig. 3a**). With a prior matrix and a normalized
233 gene expression matrix from hundreds of B-ALL specific patient samples, we used the
234 Inferelator algorithm to infer regulatory interactions. Finally, to reduce the number of regulatory
235 hypotheses on TF-gene interactions and improve predictions, we tested only regulatory
236 interactions of TFs (n=138) that were significantly enriched at differentially accessible promoters
237 between *CRLF2*-High and other B-ALL patient samples **(Supplemental Fig 3a)**.

238 The second step of network inference involves estimating the activity of all TFs in our
239 network based on the cumulative effect of each TF on its target genes[29,37]. The prior matrix
240 represents a list of potential TF-gene interactions derived from ATAC-TF-motif analysis and the
241 activity of each TF can be estimated by taking the pseudo-inverse of the prior multiplied by the
242 gene expression matrix (**Fig. 3a**). Thus, transcription factor activities were estimated using the
243 ATAC-seq motif derived priors and the gene expression matrix obtained from the TARGET
244 database (**Fig. 3a**). Finally, gene expression was modeled as a weighted sum of its activities
245 using regression with regularization (see methods section for details). The output is a matrix
246 where each row represents a TF-gene interaction, with a β parameter that corresponds to the
247 magnitude and direction of a particular interaction and a computed confidence score (see
248 methods section for details).

249 Using the ATAC–motif prior, the performance of our model selection within the
250 Inferelator was evaluated by applying a 10-fold cross validation technique. Specifically, we split
251 the prior into 10 equal sized sets. One set was retained as the gold standard to test the model,

252 while the remaining 9 sets were used as the prior. The cross-validation procedure was repeated
253 10 times, until each of the 10 partitions was used exactly once as the gold standard. As a
254 negative control, we employed the same 10 fold cross-validation strategy after randomly
255 shuffling the prior. We computed the area under the precision-recall curve (AUPR) for each of
256 the 10 iterations and compared the results between the prior and the shuffled prior. Overall,
257 AUPR were significantly higher using the ATAC-seq derived motif prior compared to the
258 randomly shuffled prior (**Supplemental Fig 3b**). Thus, the final network was inferred using the
259 ATAC-seq derived motif prior and the number of significant regulatory interactions was limited to
260 TF-gene interactions with combined confidences > 0.9 (high-confidence interactions). This
261 generated a B-ALL specific regulatory network involving 135 TFs (that may be important
262 regulators of *CRLF2*-High gene signature) and 8,731 high confidence patient specific TF-gene
263 interactions (**Fig. 3a**).
264

265 **Significant Transcription Factors altered by *CRLF2* overexpression**

266 To identify TFs affected by *CRLF2* overexpression, we reapplied the TF activity
267 estimation strategy described above to estimate activity across the 30 *CRLF2*-High and other B-
268 ALL samples. By assigning the inferred 8,731 patient-specific TF-gene interactions as priors
269 with the normalized gene expression matrix including all 30 primary patient samples, we
270 estimated an activity matrix of all 135 TFs. Next, we evaluated TFA estimates using PCA
271 analysis across the 30 samples and demonstrated a clear separation of *CRLF2*-High and Low
272 patient samples (**Fig. 3b**). To define the top TFs that explain the variance associated with
273 overexpression of *CRLF2*, we extracted and ranked the absolute value of the PC1 values for
274 each TF (**Supplemental 4a)**. As a secondary means to identify TFs altered at the activity level,
275 we computed the mean activity level of each TF between *CRLF2*-High and Low samples and

276 tested for statistical difference**.** To narrow the list of potential TFs altered as a result of *CRLF2*
277 overexpression, we ranked the most highly variable TFs and retained those with |PC1| > 0.075,
278 as well as TFs with significant differences in mean activity level with an adjusted p-value 0.001.
279 This resulted in 36 significant TFs as highlighted in the volcano plot in **Fig. 3c**. Boxplots
280 depicting highly variable TFs (n=36) with significant differential mean activities are represented
281 in **Supplemental Fig 4b**. As a result, we defined 36 significant TF regulators predicted to
282 regulate 2,410 gene targets from the inferred B-ALL regulatory network previously described,
283 with the number of targets for each TF shown in **Supplemental Fig 4c**. We note that many TFs
284 (FOXM1[38], ETS2[39,40], BCL11A[41], FOXO1[42], etc.) with significantly altered activity are implicated
285 in cancer and could therefore potentially contribute to tumorigenesis in *CRLF2*-High B-ALL
286 patients. Furthermore, 6 of the 36 significant TFs (*ETS2, SRY, FOXO1, EGR1, MEF2D, KLF5*)
287 exhibit a statistically significant difference in mRNA expression between the two patient groups
288 (**Supplemental Fig. 4d**). According to both transcriptional and predicted activity levels, these
289 TFs represent robust candidates that could be important downstream effectors of the *CRLF2*-
290 mediated signaling cascade driving leukemogenesis.
291
292 **A *CRLF2*-associated sub-network of altered TFs and their differentially expressed targets**

293 To filter regulatory interactions to a specific *CRLF2*-High sub-network, we computed the
294 number of gene targets that were differentially expressed (542/2410) in *CRLF2*-High versus
295 *CRLF2*-low patient samples (**Fig. 4a**). Ingenuity pathway analysis was performed on the 542
296 differentially expressed gene targets in the *CRLF2*-High associated sub-network. This
297 generated 22 significant pathways (**Fig. 4b**) including the activation of the canonical PI3K
298 pathway (**Fig. 4a**). The majority of the gene targets are involved in more than one signaling
299 pathway and many of these pathways are important in adaptive immunity and inflammatory
300 responses.

301 To define a set of genes in the *CRLF2*-High associated sub-network that could have the
302 highest potential as therapeutic targets, we turned to patient-derived cell lines to identify robust
303 changes across both model systems. The patient-derived cell lines used in our analysis were
304 MHH-CALL-4[43] (CALL) and MUTZ5[44] (MUTZ) that harbor *IGH-CRLF2* translocations leading to
305 *CRLF2* overexpression, and a non-translocated B-ALL pre-B leukemic cell line, SMS-SB[45]
306 (SMS). As seen in the RNA-seq tracks of **Supplementary Fig. 5a**, *CRLF2* is clearly
307 overexpressed in the translocated CALL and MUTZ cell lines, compared to non-translocated
308 SMS. Principal component analysis of cell line RNA-seq samples (**Supplementary Fig. 5b**)
309 indicated that the majority of the variance (71%) lies between *CRLF2*-High cell lines and SMS
310 cell lines, while about 26% of variance separated the two *CRLF2*-High cell lines. Thus the PCA
311 analysis demonstrates overexpression of *CRLF2* is the major difference between the two
312 conditions, consistent with what was observed in patient samples.

313 Differential gene expression analysis of CALL versus SMS (1,631 DE genes) and MUTZ
314 versus SMS (1,484 DE genes) identified thousands of differentially expressed genes
315 (**Supplementary Fig. 5c**), with roughly equivalent numbers of up and down-regulated genes in
316 each case. The number of overlapping differentially expressed genes is shown in
317 **Supplementary Fig. 5d**. As shown in **Supplementary Fig. 5e,** the $\log_2$ fold change of
318 (CALL/SMS) and (MUTZ/SMS) demonstrated that about 97% of the genes were in convergent

319 orientation (561 up-regulated, 353 down-regulated). We compared the gene targets in the
320 *CRLF2*-associated regulatory sub-network with the convergent differentially expressed genes in
321 cell lines and identified 67 significant convergent transcriptional alterations that were conserved
322 across *CRLF2*-High patient and cell line samples. This is shown in **Figure 4c** by the $\log_2$ fold
323 change of all 67 convergent differentially expressed genes in the patients and each pairwise cell
324 line comparison (CALL versus SMS, and MUTZ versus SMS). Of the 67 gene targets, 84% are
325 up-regulated in *CRLF2*-High samples including *PIK3CD, DPEP1, PTPN7, TNFRSF13C*
326 *(BAFFR)* and Class II major histocompatibility complex (MHC) genes. Previous studies have
327 implicated the majority of these genes in hematologic malignancies including B-ALL[46-51] but their
328 affect specifically in *CRLF2*-overexpressing B-ALL is not known. Furthermore, thirteen of these
329 genes have available inhibitors (**Supplemental Table 3**).
330
331 **Validating Inferred Gene Targets of TFs significantly altered by *CRLF2* overexpression**
332 To support our network-based approach in identifying TF-gene regulatory interactions in
333 leukemic cells, we sought to validate our predictions of interactions involving TFs using publicly
334 available data in similarly related cells. We collected ENCODE data to support TF-gene
335 associations involving 9 significant TFs. The experiments analyzed include CRISPR
336 interference (CRISPRi) targeting of FOXM1 in myelogenous leukemic cells (K562), siRNA
337 targeting of MAZ and E2F6 in K562 cells, and ChIP-seq for 6 significant TFs (BCL11A, ETS2,
338 EGR1, PBX2, IRF1, TBP) in K562 cells and a B-lymphocyte derived cell line (GM12878).
339 First, we computed the number of gene targets we inferred for each of the 9 TFs (**Figure**
340 **5a**). To validate some of the predicted gene targets of FOXM1, we compared RNA-seq samples
341 in K562 cells treated with CRISPRi targeting of FOXM1 versus non-targeted cells. A PCA of
342 these samples distinctly separates the FOXM1 CRISPR targeted samples from the non-
343 targeting control samples (**Figure 5b**). DESeq2 was applied was used to examine differentially
344 expressed genes associated with FOXM1 targeting. These were overlapped with the network's

345 predicted gene targets of FOXM1. Of the 123 gene targets we predicted to be regulated by
346 FOXM1, 50 (40%) had a significant change in their expression upon FOXM1 CRISPRi targeting
347 including *CRLF2* itself (**Figure 5c**). FOXM1 is a forkhead box transcription factor functioning
348 downstream of the PI3K/AKT/mTOR pathway, which is known to be induced in *CRLF2*-
349 overexpressing B-ALL[7,52]. It is involved in cell proliferation, DNA repair, and self-renewal.
350 Overexpression of FOXM1 has been detected not only in B-ALL[38] but also in a wide range of
351 human cancers and its overexpression is linked to poor prognosis[38,53-62].

352 To evaluate predicted gene targets of another significant TF, we identified genes altered
353 by siRNA knockdown of the E2F6 gene in K562 cells. E2F6 is one of the E2F transcription
354 factors that play distinct and overlapping roles in regulating cell cycle progression[63]. E2F
355 proteins can be transcriptional activators or repressors. In particular, E2F6, has been shown to
356 repress the transcription of known E2F target genes and is considered a dominant negative
357 inhibitor of the other E2F proteins. Yeast two-hybrid assays have determined that E2F6
358 associates with known components of the polycomb complex, suggesting a role for E2F6 in
359 recruiting the polycomb transcriptional repressor to target genes[64]. To support some the inferred
360 gene targets of E2F6 using the network based strategy in this study, we analyzed E2F6
361 targeted RNA-seq samples using siRNA versus non-targeted controls. A PCA analysis
362 confirmed expected clustering of replicates for E2F6 targeted and control samples (**Figure 5d**).
363 Differentially expressed genes were determined and overlapped with inferred gene targets of
364 E2F6. This analysis supported 57 of the 272 (21%) predicted E2F6 gene targets (**Figure 5e**).

365 Next, we analyzed predicted gene targets of the MAZ TF, also known as Myc-associated
366 zinc-finger protein. This TF is ubitiquously expressed in most tissues and has been shown to
367 activate a variety of genes including c-Myc, insulin, VEGF, and MYB, and repress the p53
368 protein[65-67]. Specifically, it has been shown that the kinase Akt phosphorylates MAZ, which
369 leads to the release of the MAZ TF from the p53 promoter followed by p53 transcriptional
370 activation[66]. MAZ has also recently been identified as a factor that interacts with cohesin and

371 through this connection alter gene regulation as a result of its impact on TAD structure[68]. As
372 MAZ has been shown to have a dual role in both activation and repression of cancer-related
373 genes, it's role in different cancer types can vary greatly depending on its target genes. In this
374 particular study, we have predicted significant B-ALL specific regulatory interactions between
375 MAZ and 26 gene targets. To provide evidence supporting these predictions, we analyzed
376 siRNA knockdown of MAZ in K562 RNA-seq samples compared to control samples. A PCA on
377 MAZ knockdown and control K562 samples indicated reproducible replicates that cluster
378 according to their condition (**Figure 5f).** Genes that were differentially expressed were analyzed
379 and overlapped with predicted MAZ gene targets, resulting in 15% of predicted gene targets'
380 expression significantly altered by siRNA knockdown of MAZ (**Figure 5g).**

381 Finally, to support TF-gene regulatory interactions of other significant factors, we
382 downloaded available ENCODE optimal IDR (Irreproducible Discovery Rate) peaks for 6
383 important TFs (BCL11A, ETS2, EGR1, PBX2, IRF1, TBP) in K562 and GM12878 cell lines.
384 Optimal IDR peaks represent the most highly reproducible peaks across replicates. The aim
385 here was to delineate potential gene targets of each TF by determining binding sites according
386 to significant and reproducible ChIP-seq peaks at promoters. Thus, ChIP-seeker was applied to
387 annotate the optimal IDR peak sets of each TF to genes, using the same threshold applied to
388 generate TF-gene priors as previously described (20 KB window upstream of the TSS), the
389 number of genes associated with at least one ChIP-seq peak for each TF is shown in **Figure**
390 **5h**. For each individual TF of interest, we overlapped the network inferred gene targets of that
391 TF with the genes associated with ChIP-seq binding. Overall, we were able to validate 40.1% of
392 BCL11A gene targets, 69% of EGR1 gene targets, 6.1% of ETS2 gene targets, 26.3% of IRF1
393 gene targets, 57% PBX2 gene targets, and 47.8% of TBP gene targets that we infer using the
394 network-based approach (**Figure 5i**). Finally, individual hyper-geometric tests were performed
395 for each experiment; to test the significance of the proportion of validated gene targets
396 compared to random. The proportion of validated gene targets was significant for almost all 9

397 TFs, with the exception of ETS2, which could most likely be a matter of cell-type context (**Figure**
398 **5i**).
399
400
401 **DISCUSSION**
402 Patients with B-ALL who overexpress *CRLF2* are at increased risk for refractory disease
403 and relapse. This alteration leads to the activation of JAK-STAT and other associated
404 pathways[3]. Available treatments include non-specific cytotoxic chemotherapies which though
405 often effective are responsible for many of the toxicities seen in these patients. The addition of
406 Tyrosine-Kinase Inhibitors and JAK inhibitors in the treatment of leukemias has allowed for
407 targeted treatments but these treatments also affect the biology of healthy cells. Furthermore,
408 the use of *CRLF2*-targeted CAR T cells shows great promise in the eradication of the cancer,
409 yet limitations and toxicities associated with this treatment have yet to be studied in patients.
410 Thus, it is important to more deeply investigate the regulatory control underlying *CRLF2*-
411 overexpressing leukemia to identify and evaluate alternate gene therapeutic targets for tailored
412 treatment.
413 In this work, we sought to better understand the impact of *CRLF2* overexpression on
414 leukemogenesis, with the aim of delineating the regulatory interactions for patient-specific
415 *CRLF2*-High B-ALL. We analyzed RNA-seq from *CRLF2*-High and Other B-ALL patient samples
416 and identified hundreds of differentially expressed genes. We subsequently analyzed ATAC-seq
417 data to evaluate the effects of this genetic alteration on DNA accessibility. We found
418 accessibility to be altered across the genome with an enrichment of changes localized to
419 promoter regions. Only a small proportion of these altered promoter regions are linked with
420 gene expression changes.
421 To systematically annotate regulatory interactions, we inferred putative binding of
422 specific TF motifs at all ATAC-seq peaks found at the promoters of genes in the genome.

423 Leveraging hundreds of available B-ALL RNA-seq samples from the TARGET database along
424 with prior knowledge of TF-motifs at accessible promoters allowed us to infer a B-ALL specific
425 regulatory network involving TF motifs (135) enriched at differentially accessible promoters.
426 Deeper investigation of the TF regulators and robust differential gene targets specific to the
427 *CRLF2*-High sub-network identified a candidate list of potential therapeutic targets.

428 *PIK3CD*, one of the significantly overexpressed candidates identified in *CRLF2*-High
429 patients, encodes a class I phosphoinositide-3 kinase (PI3Ks), which is highly enriched in
430 leukocytes and known as p110δ. Up-regulation of this gene has been demonstrated to occur in
431 T-cell [46] acute lymphoblastic leukemia and it has emerged as a therapeutic target. Specifically,
432 the use of a p110δ inhibitor has led to reduced proliferation and apoptosis in T-ALL cell lines[46].
433 Furthermore, this gene target has been similarly implicated in Philadelphia chromosome–like
434 acute lymphoblastic leukemia (Ph-like ALL), another high-risk B-ALL subtype correlated with
435 poor prognosis[14]. *CRLF2* overexpression occurs in about 50% of Ph-like ALL cases. Using
436 patient-derived xenograft (PDX) models of childhood Ph-like ALL, Tasian et al. demonstrate the
437 therapeutic efficacy of Idelalisib, a PI3Kδ inhibitor in vivo[14]. That PIK3CD has been previously
438 implicated in *CRLF2*-overexpressing B-ALL supports our approach in identifying relevant
439 *CRLF2*-associated gene targets.

440 Another gene target up-regulated in *CRLF2*-High patients is *GAB1*. This gene encodes
441 an adapter protein that recruits proteins, including PI3K to the plasma membrane to propagate
442 signals for many important biological processes such as cell proliferation, motility, and
443 erythrocyte development. *GAB1* proteins lack enzymatic activity, but are phosphorylated at
444 tyrosine residues via interaction with PI3K, and this association is essential for activation of the
445 PI3K/AKT and MAPK/ERK pathways[69]. Up-regulation of *GAB1* has been linked to breast cancer
446 progression[48] and implicated in BCR-ABL positive ALL cells[47]. Previous analysis of B-ALL adult
447 patients with the BCR-ABL alteration versus BCR-ABL–negative adult ALL patients, not only
448 identified overexpression of *GAB1* but also up-regulation of several class II major

449 histocompatibility complex (MHC) genes and their trans activator *CIITA*[47]. These results are
450 similarly reproduced in our own data demonstrating conserved co-expression of *GAB1*, *CIITA,*
451 *HLA-DQA1, HLA-DQB1,* and *HLA-DRB1* across patients and cell lines. In addition, we
452 determined that 4 out of 5 of these genes (*GAB1*, *CIITA, HLA-DQA1, HLA-DQB1)* are predicted
453 to be gene targets of the BCL11A transcription factor. BCL11A is a zinc finger protein that is
454 expressed in hematopoietic cells and in the brain and whose presence is linked to
455 hematological malignancies[41,70]. This TF has been shown to play an important role in lymphoid
456 development. BCL11A expression in adult mouse is found in most hematopoietic cells but
457 enriched in B cells, early T cell progenitors, common lymphoid progenitors (CLPs) and
458 hematopoietic stem cells (HSCs). The deletion of BCL11A leads to early B-cell and CLP
459 apoptosis and impairs the development of HSCs into B, T, and natural killer (NK) cells[71].
460 BCL11A is a key regulator of fetal-to-adult hemoglobin switching. This regulator is also known to
461 interact with the chromatin remodeling SWI/SNF complex and the nucleosome remodeling and
462 deacetylase (NuRD) complex.[72]. The analysis described earlier, associating BCL11A ChIP-seq
463 binding sites to genes in GM12878 cells, validated 56 of BCL11A's predicted gene targets,
464 including overexpressed *GAB1*, *CIITA, HLA-DQA1, HLA-DQB1,* and *HLA-DRB1* in both patients
465 and cell lines. Another candidate gene target of BCL11A, validated by ChIP-seq binding, is
466 *DPEP1.* As a zinc-dependent peptidase, *DPEP1* is important for metabolism of the antioxidant
467 glutathione and was recently linked to relapse in B-ALL. Specifically, high levels of this gene
468 were linked with a higher incidence of relapse and worse overall survival[73].

469 *GAB1* is also one of the few gene targets that we predict to be regulated by two
470 significantly altered TFs, BCL11A and PBX2. The pre-B-cell leukemia transcription factor 2,
471 PBX2 is a ubiquitously expressed protein and can regulate gene expression and effect
472 processes such as cell proliferation and differentiation[74]. It has also been shown to work as a
473 cofactor with the HOXA9 protein[75]. Knockdown of PBX2 leads to increased apoptosis in
474 adenocarcinoma and esophageal squamous cell carcinoma cancer cell lines[76]. PBX2 is also an

475 inferred regulator of the down-regulated *PTPN7* gene in *CRLF2*-overexpressing patients and
476 cell lines. This gene encodes a protein tyrosine phosphatase that is mainly expressed in
477 hematopoietic cells and known to negatively regulate the activation of ERK and MAPK
478 kinases[77]. Overexpression of *PTPN7* in T-cells down-regulates ERK signaling and reduces T-
479 cell activation and proliferation[78]. Thus, *PTPN7* represents another strong candidate gene target
480 as it can act as a negative regulator of one the canonical signaling pathways downstream of
481 *CRLF2*.

482 The up-regulation of *TNFRSF13C*, has also been linked to relapse in B-cell acute
483 lymphoblastic leukemia. *TNFRSF13C* encodes the receptor for B-cell activating factor (BAFFR)
484 and is important for B-cell maturation and survival. Expression of *TNFRSF13C* is primarily
485 detected in primary B-cell malignancies and B-cell related organs and absent in other healthy
486 related tissues[79,80]. There is evidence suggesting the expression of this receptor plays a role in
487 relapse as well as persistence of leukemic cells after early treatment[80]. Current drugs available
488 to target the BAFFR receptor include the Anti–BAFF-R antibody VAY-736[81]. In addition, a CAR-
489 based strategy has recently been engineered to target this receptor. Thus, *TNFRSF13C*
490 represents a potential target for *CRLF2*-overexpressing leukemias.

491 The network-driven approach also identified a number of significant TF regulator motifs
492 including ETS2[40], FOXO1[42], EGR1[82], and FOXM1[38,55,56], which are implicated in hematological
493 malignancies. FOXM1 could be an important regulator in *CRLF2*-overexpressing cells due to its
494 crucial role in cell proliferation and its implication in various cancer types, as described earlier.
495 Furthermore, our investigations predict that FOXM1 regulates *CRLF2* itself. This is interesting,
496 as FOXM1 is a known regulator functioning downstream of *CRLF2*-associated PI3K/AKT
497 pathway, yet it was not known that FOXM1 could regulate *CRLF2*.

498 Another candidate regulator, ETS2, a member of the *Ets* family of transcription factors, is
499 involved in cell proliferation and differentiation, and is a known target of the RAS/MAPK
500 signaling pathway[83]. In this study, ETS2 is differentially expressed and predicted to regulate the

501 aforementioned gene target *TNFRSF13C* or BAFFR. In AML, overexpression of ETS2 has been
502 shown to be associated with shorter overall survival and be a predictor of poor prognosis[39].
503 Analysis of overexpressed ETS2 in AML is associated with co-expression of *SOCS2* and *TCF4*,
504 both of which are significantly up-regulated in *CRLF2*-High B-ALL patient samples. *A*s
505 mentioned previously, *SOCS2* is induced upon cytokine signaling. *TCF4*, also known as
506 *TCF7L2*, is a transcription factor that plays an important role in the Wnt signaling pathway and
507 its overexpression is required for proliferation and survival of AML cells[84]. Indeed, the results of
508 our present study identified *TCF4* as part of the *CRLF2*-associated sub-network and it is
509 overexpressed in both primary patients and patient derived cell lines. Given the role of *TCF4* in
510 the Wnt signaling pathway and its link to poor clinical outcome in AML, this gene represents
511 another putative gene target in *CRLF2*-overexpressing B-ALL.

512 FOXO1, another significantly altered TF, is one of the FOXO transcription factors
513 regulated by the PI3K/AKT signaling pathway. FOXO TFs are mostly considered as tumor
514 suppressors given their ability to inhibit cancer cell growth. Yet there is contrasting evidence for
515 their activation supporting tumor progression and inducing drug resistance[85]. In particular, the
516 TF FOXO1 plays a vital role in regulating proliferation and cell survival during B-cell
517 differentiation and it's activity, has been shown to be essential in B-cell precursor acute
518 lymphoblastic leukemia[42]. In this specific study in B-ALL, Wang et al. inhibited FOXO1 and
519 demonstrate reduced leukemic activity in cell lines, primary patients, and xenograft models[42].

520 The Early Growth Response 1 **(**EGR1**)** TF represents another candidate TF that is not
521 only significantly altered at the gene expression level but also predicted to have a change in
522 activity. This TF is induced in response to B cell receptor (BCR) signaling and mediated by the
523 Ras/Raf-1/MAPK pathway. Studies have also shown that EGR1 can promote differentiation in
524 pre-B cells[86]. High levels of EGR1 have been linked to human diffuse large B lymphoma cells
525 suggesting a role for EGR1 in B lymphoma cell growth[82]. In addition to previous evidence
526 supporting a role for FOXM1, ETS2, BCL11A, PBX2, EGR1, and FOXO1 in other malignancies,

527 the results of our analysis now implicate these TFs in *CRLF2*-overexpressing leukemia. We
528 speculate that downstream of *CRLF2*-mediated signaling, there are alterations to the
529 accessibility landscape that may be influencing TF binding and thereby deregulating
530 transcriptional programs. We have identified a set of TFs and their respect gene targets that we
531 propose may be important factors to consider in *CRLF2*-overexpressing leukemia (**Fig. 6a**).
532 Finally, using CRISPRi and siRNA RNA-seq data for FOXM1, E2F6, and MAZ, as well as ChIP-
533 seq for 6 other TFs from ENCODE, it was possible to validate a proportion of our predictions
534 linking these TFs and their predicted gene targets.

535 In summary, we have investigated the transcriptional impact of *CRLF2* overexpression in
536 a high-risk subset of B-ALL patients. Using an integrative approach, we derived regulatory
537 interactions that have enabled the identification of potential candidates for targeted therapies in
538 B-ALL patients with *CRLF2* overexpression. *PIK3CD, GAB1, DPEP1, TNFRSF13C, TFC4,*
539 *PTPN7, BCL11A, FOXM1, ETS2, EGR1, PBX2,* and *FOXO1* are amongst the most interesting
540 candidates as there is evidence supporting their role in hematological malignancies. The
541 strategy we have used here can further be adapted to elucidate important regulators and gene
542 targets responsible for additional subsets of B-ALL and other challenging malignancies.

543
544
545 **METHODS**
546
547 **Cell Culture**

548 The MUTZ5 (RRID:CVCL_1873) and MHH-CALL-4 (RRID:CVCL_1410) human B-cell leukemia
549 cell lines carrying CRLF2-High translocation were obtained, as well as the SMS-SB
550 (RRID:CVCL_AQ30) human B-cell leukemia control cell line. All cells were maintained in
551 RPMI1640 supplemented with 20% FBS and 1% penicillin-streptomycin under 5% CO2 at 37
552 degrees. Ficoll-enriched, cryopreserved bone marrow samples were obtained from the
553 Children's Oncology Group (COG) from pediatric patients with B-precursor ALL from biology
554 protocols AALL03B1 and AALL05B1. Both *CRLF2*-HIGH and control patient samples were

555 used. All subjects (or their parents) provided written consent for banking and future research
556 use of these specimens in accordance with the regulations of the institutional review boards of
557 all participating institutions.
558
559 **RNA-seq**
560 RNA was extracted using the RNeasy plus kit from QIAGEN. For the cell lines, ribosomal
561 transcripts were depleted using the Illumina® Ribo Zero Module and for the patients, poly-
562 adenylated transcripts were positively selected using the NEBNext® Poly(A) mRNA Magnetic
563 Isolation Module, following the respective kit procedure. Libraries were prepared according to
564 the directional RNA-seq dUTP method adapted from
565 http://waspsystem.einstein.yu.edu/wiki/index.php/Protocol:directional_WholeTranscript_seq that
566 preserves information about transcriptional direction. Sequencing was performed with Illumina
567 Hi-Seq 2500 using 50 cycles paired-end mode.
568
569 **ATAC-seq**
570 Cell were counted to collect 50,000 cells per sample. The assay was performed as described
571 previously[87]. Cells were washed in cold PBS and resuspended in 50 µl of cold lysis buffer (10
572 mM Tris-HCl, pH 7.4, 10 mM NaCl, 3mM MgCl2, 0.1% IGEPAL CA-630). The tagmentation
573 reaction was performed in 25 µl of TD buffer (Illumina Cat #FC-121-1030), 2.5 µl Nextera Tn5
574 Transposase, and 22.5 µl of Nuclease Free H2O at 37oC for 30 min. DNA was purified on a
575 column with the Qiagen Mini Elute kit, eluted in 10 µl H2O. Purified DNA (10 µl) was combined
576 with 10 µl of H2O, 2.5 µl of each primer at 25 mM and 25 µl of NEB Next PCR master mix. DNA
577 was amplified for 5 cycles and a monitored quantitative PCR was performed to determine the
578 number of extra cycles needed as per the original ATAC-seq protocol[87]. DNA was purified on a
579 column with the Qiagen Mini Elute kit. Samples were quantified using Tapestation bioanalyzer

580 (Agilent) and the KAPA Library Quantification Kit and sequenced on the Illumina Hi-Seq 2000
581 using 50 cycles paired-end mode.
582
583 **QUANTIFICATION AND STATISTICAL ANALYSIS**
584 **RNA-seq analysis in *CRLF2*-High and other B-ALL patient cohort**
585 RNA-seq with replicates for individual patient samples were pooled. Paired-end reads were
586 mapped to the hg38 genome using TopHat2[88] (parameters:–no-coverage-search–no-
587 discordant–no-mixed–b2-very-sensitive–N 1). To Counts for Refseq genes were obtained using
588 htseq-counts[89]. PCA was performed using R to visualize the clustering of the patient samples.
589 Differential analysis was performed using DESeq2[32] and differential genes were considered
590 statistically significant if they had an adjusted p-value less than 0.01 and |log2 FoldChange| >2.
591 Hierarchical clustering was performed on significant differentially expressed genes (3,586) with
592 the manhattan distance and ward.d2 clustering method, using heatmap3 R package for
593 visualization. Bigwigs were obtained for visualization on individual as well as merged bam files
594 using Deeptools[90] (parameters bamCoverage–binSize 1–normalizeUsing RPKM). Gene Set
595 Enrichment Analysis (GSEA) for pathway enrichment was performed using the default
596 parameters of the GSEA desktop application on normalized reads counts for all patient samples
597 for the 3,586 differentially expressed genes between *CRLF2*-High and other B-ALL patients.
598 See below for information for each RNA-seq sample:
599

Original Label	Source	File Name	Sample Name
CRLF2-High_1	Skok Lab	CRLF2-High_1_RNA_counts.txt	CRLF2-High_1
CRLF2-High_2	Skok Lab	CRLF2-High_2_RNA_counts.txt	CRLF2-High_2
CRLF2-High_3	Skok Lab	CRLF2-High_3_RNA_counts.txt	CRLF2-High_3

CRLF2-High_4	Skok Lab	CRLF2-High_4_RNA_counts.txt	CRLF2-High_4
CRLF2-High_5	Skok Lab	CRLF2-High_5_RNA_counts.txt	CRLF2-High_5
CRLF2-High_6	Skok Lab	CRLF2-High_6_RNA_counts.txt	CRLF2-High_6
CRLF2-High_7	Skok Lab	CRLF2-High_7_RNA_counts.txt	CRLF2-High_7
CRLF2-High_8	Skok Lab	CRLF2-High_8_RNA_counts.txt	CRLF2-High_8
CRLF2-High_9	Skok Lab	CRLF2-High_9_RNA_counts.txt	CRLF2-High_9
CRLF2-High_10	Skok Lab	CRLF2-High_10_RNA_counts.txt	CRLF2-High_10
CRLF2-High_11	Skok Lab	CRLF2-High_11_RNA_counts.txt	CRLF2-High_11
CRLF2-High_12	Skok Lab	CRLF2-High_12_RNA_counts.txt	CRLF2-High_12
SRR457636	TARGET	CRLF2-High_13_RNA_counts.txt	CRLF2-High_13
SRR457642	TARGET	CRLF2-High_14_RNA_counts.txt	CRLF2-High_14
SRR457653	TARGET	CRLF2-High_15_RNA_counts.txt	CRLF2-High_15
SRR3162137	TARGET	BALL_1_RNA_counts.txt	BALL_1
SRR3162141	TARGET	BALL_2_RNA_counts.txt	BALL_2
SRR3162143	TARGET	BALL_3_RNA_counts.txt	BALL_3
SRR3162144	TARGET	BALL_4_RNA_counts.txt	BALL_4
SRR3162148	TARGET	BALL_5_RNA_counts.txt	BALL_5
SRR3162151	TARGET	BALL_6_RNA_counts.txt	BALL_6
SRR3162166	TARGET	BALL_7_RNA_counts.txt	BALL_7
SRR3162280	TARGET	BALL_8_RNA_counts.txt	BALL_8
SRR3162282	TARGET	BALL_9_RNA_counts.txt	BALL_9

SRR3162293	TARGET	BALL_10_RNA_counts.txt	BALL_10
SRR3162301	TARGET	BALL_11_RNA_counts.txt	BALL_11
SRR3162304	TARGET	BALL_12_RNA_counts.txt	BALL_12
SRR3162313	TARGET	BALL_13_RNA_counts.txt	BALL_13
SRR3162316	TARGET	BALL_14_RNA_counts.txt	BALL_14
SRR3162374	TARGET	BALL_15_RNA_counts.txt	BALL_15

ATAC-seq analysis in patient samples

ATAC-seq primary patient samples reads were mapped against the hg38 reference genome using Bowtie2[91]. ATAC-seq replicates for individual patient samples were pooled. ATAC-seq peaks were called using MACS2. A reference list of peaks or peakome representing all possible ATAC-seq peaks across patient samples was compiled by taking the union of all peaks and merged overlapping peaks. This resulted in a peakome of about 115,457 peaks. Differential analysis was performed using DESeq2[32] and differentially accessible regions were considered significant if they had an adjusted p-value < 0.01 and a |log2 fold change| >1. Hierarchical clustering was performed on significant differential ATAC-seq peaks (1678) with euclidean distance and complete clustering method with pheatmap R package. Genomic annotation of significant differential ATAC-seq peaks was done using ChIPseeker[92] with a 3kb window on either side of the TSS, to associate promoter peaks. Bigwigs were obtained for visualization using Deeptools/2.3.3[90] (parameters bamCoverage --binSize 1 --normalizeUsing RPKM). Heatmaps indicating average ATAC-signal at differentially expressed genes were generated using Deeptools.

RNA-seq analysis in patient derived cell lines

619 Paired-end reads were mapped to the hg38 genome using TopHat2[88] (parameters:–no-
620 coverage-search–no-discordant–no-mixed–b2-very-sensitive–N 1). Counts for genes were
621 obtained using htseq-counts[89]. Differential analysis was performed using DESeq2[32] and
622 differential genes were considered statistically significant if they had an adjusted p-value less
623 than 0.01 and |log2 FoldChange| >2.
624

625 **TARGET RNA-seq analysis of 868 primary patient samples**

626 We downloaded 868 B-ALL patient samples from the TARGET database and samples
627 were analyzed using the sns workflow (https://github.com/igordot/sns) to align and generate
628 counts for genes. Specifically, paired-end reads were mapped to the hg38 genome from
629 GENCODE using STAR aligner[93] and counts for the 57,316 GENCODE genes (includes coding
630 genes, lncRNAs and pseudogenes) were obtained. Data was normalized using DESeq2[32].
631

632 **Identifying the most likely TF regulators used for network inference**

633 To generate a list of candidate TF regulators, we identified a list of enriched TF motifs at
634 differentially expressed ATAC-seq peaks at promoters (793) previously annotated (**Figure 5e**) in
635 *CRLF2*-High versus Other B-ALL patients using Analysis of motif enrichment (AME[35]) to identify
636 enriched TF motif that are present in the Cis-BP[94] motif database. AME scores a set of regions
637 with a motif compared to a control sequence. Here we used randomly shuffled input sequences
638 as control sequences and used the one-tailed Fisher's Exact test to test for motif enrichment. TF
639 motifs with an adjusted p-value< $1e^{-13}$ were considered enriched TF motifs at promoters with
640 differentially accessible ATAC-seq peaks, which led to a list of 138 TFs. This allows us to limit
641 the number of TF-gene regulatory hypothesis tested.

642

643 **Estimating transcription factor activities (TFA)**

644 To generate the prior matrix from the *CRLF2*-high patient cohort, human TF binding
645 motifs (PWMs) were downloaded from the Cis-BP[94] motif database. Next, we used FIMO[95] to
646 scan for TF motifs at all ATAC-seq peaks (union of all ATAC-seq peaks in *CRLF2*-High cohort)
647 20kb upstream of any gene TSS. TF motifs found at each 20kb window per gene with a p-value
648 < 0.0001 were counted. . TF motifs were aggregated across all ATAC-seq peaks for each gene.
649 For each TF motif-gene association, a score, a p-value and an adjusted p-value was computed.
650 Only TF-gene associations that had an adjusted p-value less than 0.01 were retained.

651 To estimate activity, first DESeq2-normalized TARGET expression data was transposed
652 into matrix ***X***, in which columns are individual patient samples and rows are genes. ***P*** is the TF-
653 gene matrix of known prior regulatory interactions between transcription factors (columns) and
654 genes (rows). $\boldsymbol{P}_{i,k}$ is zero if there is no known regulatory interaction between transcription factor
655 *k* and gene *i.* ***A*** is the activity matrix, where the columns are the individual samples as in ***X*** and
656 rows are the TFs. We model the expression of gene *i* in individual samples *j* as a linear
657 combination of the activities of each TF, *k*, in condition *j.*

$$X_{i,j} = \sum_{k \in TFs} P_{i,k} \, A_{k,j}$$

658 This means that we use the known targets of a transcription factor to derive its activity.
659 The system of linear equations above lacks a unique solution, as there are more equations than
660 unknowns. Hence, to compute a "best fit" (least squares) to the system of linear equations
661 above that lacks a unique solution, we can compute the pseudo-inverse of the prior P^{-1}
662 multiplied by the expression matrix *X* to approximate $\hat{A}$:

$$\hat{\mathrm{A}} \approx P^{-1} X$$

663 If a transcription factor has no prior targets present in ***P***, we use the expression of that
664 transcription factor as a proxy for its activity.

665 **B-ALL network inference using (Bayesian Best Subset Regression-Inferelator)**

666 We use a bayesian best-subset regression (BBSR) method, previously described[36]
667 within the current Inferelator algorithm[25,26]. At steady state, we model the expression of a gene i
668 in individual cell j as a linear combination of the activities of its TF regulators in individual
669 samples j :

$$X_{i,j} = \sum_{k \in TFs} \beta_{i,k} A_{k,j}$$

670 The goal of the network inference procedure is to find a sparse solution for β, in which
671 non-zero entries define both the strength and direction (activation or repression) of a regulatory
672 relationship. This is because we expect a limited number of transcription factors to regulate a
673 particular gene. We select the model with the lowest Bayesian Information Criterion, which adds
674 a penalty term to the training error to account for model complexity and thereby reduce
675 generalization error. After this step, the output is a matrix of inferred regression parameters β,
676 where each entry corresponds to a regulatory relationship between transcription factor k and
677 gene i. Final TF-gene interactions were retained if they had a combined confidence > 0.9 and a
678 precision > 0.3, which resulted in 8,731 regulatory interactions between 135 TFs and 6,645
679 unique gene targets. Networks were visualized using jp_gene_viz, an interactive interface,
680 designed on iPython. Software is available at https://github.com/simonsfoundation/jp_gene_viz.

681

682 **Evaluating Performance of the model**

683 Performance of our model selection within the Inferelator is evaluated by applying a 10-
684 fold cross validation technique using the ATAC-motif prior. The prior matrix was split into 10
685 equal sized sets. One set is retained as the gold standard to test the model, while the remaining
686 9 sets are used as the prior. The cross-validation procedure is repeated 10 times, until each of
687 the 10 partitions is used exactly once as the gold standard. To generate a negative control, we

688 randomly shuffle the prior and employ the same 10 fold cross-validation strategy. Next, we
689 compute the area under the precision-recall curve (AUPR) for each of the 10 iterations and
690 compare the results between the prior and the shuffled prior. To test for a significant increase in
691 AUPR values using the ATAC-motif prior compared to a shuffled prior across the 10 iterations,
692 we applied a paired t-test (p-value=$4.5e^{-5}$).

693 in AUPR values the Overall, AUPR were significantly higher using the ATAC-seq
694 derived motif prior compared to the randomly shuffled prior (**Supplemental Fig 4b**). Thus, the
695 final network was inferred using the ATAC-seq derived motif prior and the number of significant
696 regulatory interactions was limited to TF-gene interactions with combined confidences > 0.9
697 (high-confidence interactions). This generated a B-ALL specific regulatory network involving 135
698 TFs (that may be important regulators of *CRLF2*-High gene signature) and 8,731 high
699 confidence patient specific TF-gene interactions (**Fig. 5b**).

700
701
702 **Estimating Transcription Factor Activity in *CRLF2*-High cohort**

703 The B-ALL network was inferred as described above, but to approximate activity of 135
704 TFs in *CRLF2*-High cohort, we now use the inferred B-ALL network as prior information of TF-
705 gene interaction and gene expression the cohort to estimate activity. Activity values were
706 calculated for each *CRLF2*-High and other B-ALL patient samples. To identify the most likely
707 TFs altered as a result of *CRLF2* overexpression, we used to metrics to define this set of TFs.
708 First, we performed PCA analysis on the activity matrix of 135 TFs. The absolute PC1 values for
709 each TF were computed and ranked to identify the most highly variable TFs that best separate
710 *CRLF2*-High and other B-ALL patient samples, we randomly selected the absolute value of the
711 PC1 score > 0.75 as the most highly variable TFs. Next, we calculated the average TFA for
712 these TFs and a t-test was used to identify TFs with a significant difference in mean estimated
713 TFA between the two conditions (adjusted p-value < 0.001). As a result, we identify 36 TFs that
714 had a significant difference in mean estimated TFA and those with a |PC1| > 0.75.

715

716 **Determining the *CRLF2*-associated sub-network affected by *CRLF2* overexpression**

717 Using the inferred B-ALL regulatory interactions, we extract the subset of differentially
718 expressed genes (542) regulated by the 36 significant TFs to derive the *CRLF2*-associated sub-
719 network. Pathway analysis of these genes (Ingenuity Pathway Analysis) resulted in 22
720 significant pathways ($-\log_{10}$(B-H p-value) > 1.3 and a |z-score| >1). Differentially expressed
721 gene targets in the CRLF2-associated sub-network were overlapped with convergent
722 differentially expressed genes in patient derived cell-lines. This resulted in 67 gene targets
723 within the *CRLF2*-associated subnetwork that are robust and convergently differentially
724 expressed across patient and patient derived cell line samples. All sub-networks were visualized
725 using jp_gene_viz (https://github.com/simonsfoundation/jp_gene_viz)

726

727

728 **Validating inferred gene targets with ENCODE CRISPRi and siRNA RNA-seq samples**

729 FOXM1 CRISPRi duplicate RNA-seq samples were downloaded from ENCSR701TVL
730 experiment. Non-targeting control samples were downloaded from ENCSR095PIC experiment.
731 Samples were analyzed using the sns workflow (https://github.com/igordot/sns) to align and
732 generate counts for genes. Specifically, paired-end reads were mapped to the hg38 genome
733 from GENCODE using STAR aligner[93] and counts for the 57,316 GENCODE genes (includes
734 coding genes, lncRNAs and pseudogenes) were obtained. Differential expression analysis was
735 performed using DESeq2[32] and genes that had an adjusted p-value < 0.05 and
736 |log2FoldChange|>0.5 were considered significantly altered at the transcriptional levels. This
737 set of genes was overlapped with the number of predicted FOXM1 gene targets to identify what
738 percentage of predicted gene targets could be validated with the CRISPRi dataset. A hyper-
739 geometric test was used to test whether the number of validated gene targets was statistically

740 significant, specifically using phyper in R as follows: phyper(50, 11918, 57316 -11918, 123,
741 lower.tail = FALSE)

742 E2F6 siRNA duplicate RNA-seq samples were downloaded from ENCSR820EGA
743 experiment. Non-targeting control samples were downloaded from ENCSR095PIC experiment.
744 Samples were analyzed using the sns workflow (https://github.com/igordot/sns) to align and
745 generate counts for genes. Specifically, paired-end reads were mapped to the hg38 genome
746 from GENCODE using STAR aligner[93] and counts for the 57,316 GENCODE genes (includes
747 coding genes, lncRNAs and pseudogenes) were obtained. Differential expression analysis was
748 performed using DESeq2[32] and genes that had an adjusted p-value < 0.05 and
749 |log2FoldChange|>0.5 were considered significantly altered at the transcriptional levels. This
750 set of genes was overlapped with the number of predicted E2F6 gene targets to identify what
751 percentage of predicted gene targets could be validated with the E2F6 siRNA dataset. A hyper-
752 geometric test was used to test whether the number of validated gene targets was statistically
753 significant, specifically using phyper in R as follows: phyper(57, 3836, 57316 -3836, 272,
754 lower.tail = FALSE)

755 MAZ siRNA duplicate RNA-seq samples were downloaded from ENCSR129WCZ
756 experiment. Non-targeting control samples were downloaded from ENCSR095PIC experiment.
757 Samples were analyzed using the sns workflow (https://github.com/igordot/sns) to align and
758 generate counts for genes. Specifically, paired-end reads were mapped to the hg38 genome
759 from GENCODE using STAR aligner[93] and counts for the 57,316 GENCODE genes (includes
760 coding genes, lncRNAs and pseudogenes) were obtained. Differential expression analysis was
761 performed using DESeq2[32] and genes that had an adjusted p-value < 0.05 and
762 |log2FoldChange|>0.5 were considered significantly altered at the transcriptional levels. This
763 set of genes was overlapped with the number of predicted MAZ gene targets to identify what
764 percentage of predicted gene targets could be validated with the MAZ siRNA dataset. A hyper-
765 geometric test was used to test whether the number of validated gene targets was statistically

766 significant, specifically using phyper in R as follows: phyper(4, 2599, 57316 -2599, 26, lower.tail
767 = FALSE)
768
769
770 **Validating predicted gene targets with ENCODE ChIP-seq samples**
771 Optimal IDR ChIP-seq peaks were downloaded for 6 TFs from ENCODE from the
772 following experiments:

TF	Experiment	Cells
ETS2	ENCSR596IKD	K562
TBP	ENCSR000EHA	K562
PBX2	ENCSR263DFP	K562
BCL11A	ENCSR000BHA	GM12878
IRF1	ENCSR000EGU	K562
EGR1	ENCSR211LTF	K562

773
774 Genomic annotation of optimal IDR peaks was done using ChIPseeker[92] with a 20kb window
775 upstream of the TSS, to associate peaks to genes. The same threshold was used to generate
776 TF-gene interactions for the prior matrix used for network inference. Genes with at least one
777 optimal IDR peak were overlapped with predicted gene targets for each TF from the B-ALL
778 network. This resulted in the number of predicted gene targets supported by ChIP-seq binding
779 of each TF of interest. Hyper-geometric tests were applied to test whether the number of
780 validated gene targets was statistically significant for each TF.
781
782
783
784
785
786
787

Acknowledgements
The authors thank all members of the Skok, Bonneau, and Carroll labs for discussions. The Children's Oncology Group for providing us with the patient samples and metadata. New York School of Medicine High Performance (HPC) for technical support. Adriana Heguy and the Genome Technology Center (GTC) core for sequencing efforts. The TARGET database.

Funding
This work was supported by 1R21CA188968-01A1 and 1R35GM122515 (J.S), American Society of Hematology Research Training Award for Fellows (B.C), AACR (P.L), National Cancer Center (P.L).

Author contributions
B.C, S.B, R.B and J.S designed and managed the project. B.C, P.L, and N.E collected samples and performed experiments. S.N and W.C provided experiments. S.B performed data analyses. D.C, C.S, R.R, and A.W aided in analysis design. B.C, R.B, and J.S secured funding. S.B and J.S wrote the manuscript. R.B and J.S revised the manuscript.

Declaration of Interests
The authors declare no competing interests.

References

1 Mullighan, C. G. *et al.* Genome-wide analysis of genetic alterations in acute lymphoblastic leukaemia. *Nature* **446**, 758-764, doi:10.1038/nature05690 (2007).

2 Mullighan, C. G. *et al.* BCR-ABL1 lymphoblastic leukaemia is characterized by the deletion of Ikaros. *Nature* **453**, 110-114, doi:10.1038/nature06866 (2008).

3 Tasian, S. K. & Loh, M. L. Understanding the biology of CRLF2-overexpressing acute lymphoblastic leukemia. *Crit Rev Oncog* **16**, 13-24 (2011).

4 Mullighan, C. G. *et al.* JAK mutations in high-risk childhood acute lymphoblastic leukemia. *Proc Natl Acad Sci U S A* **106**, 9414-9418, doi:10.1073/pnas.0811761106 (2009).

5 Pandey, A. *et al.* Cloning of a receptor subunit required for signaling by thymic stromal lymphopoietin. *Nat Immunol* **1**, 59-64, doi:10.1038/76923 (2000).

6 Roll, J. D. & Reuther, G. W. CRLF2 and JAK2 in B-progenitor acute lymphoblastic leukemia: a novel association in oncogenesis. *Cancer Res* **70**, 7347-7352, doi:10.1158/0008-5472.CAN-10-1528 (2010).

825 7 Tasian, S. K. *et al.* Aberrant STAT5 and PI3K/mTOR pathway signaling occurs in human
826 CRLF2-rearranged B-precursor acute lymphoblastic leukemia. *Blood* **120**, 833-842
827 (2012).
828 8 Russell, L. J. *et al.* Characterisation of the genomic landscape of CRLF2-rearranged
829 acute lymphoblastic leukemia. *Genes Chromosomes Cancer* **56**, 363-372,
830 doi:10.1002/gcc.22439 (2017).
831 9 Russell, L. J. *et al.* Deregulated expression of cytokine receptor gene, CRLF2, is
832 involved in lymphoid transformation in B-cell precursor acute lymphoblastic leukemia.
833 *Blood* **114**, 2688-2698 (2009).
834 10 Tsai, A. G., Yoda, A., Weinstock, D. M. & Lieber, M. R.
835 t(X;14)(p22;q32)/t(Y;14)(p11;q32) CRLF2-IGH translocations from human B-lineage
836 ALLs involve CpG-type breaks at CRLF2, but CRLF2/P2RY8 intrachromosomal
837 deletions do not. *Blood* **116**, 1993-1994, doi:10.1182/blood-2010-05-286492 (2010).
838 11 Vesely, C. *et al.* Genomic and transcriptional landscape of P2RY8-CRLF2-positive
839 childhood acute lymphoblastic leukemia. *Leukemia* **31**, 1491-1501,
840 doi:10.1038/leu.2016.365 (2017).
841 12 Mullighan, C. G. *et al.* Rearrangement of CRLF2 in B-progenitor–and Down syndrome–
842 associated acute lymphoblastic leukemia. *Nature genetics* **41**, 1243-1246 (2009).
843 13 Harvey, R. C. *et al.* Rearrangement of CRLF2 is associated with mutation of JAK
844 kinases, alteration of IKZF1, Hispanic/Latino ethnicity, and a poor outcome in pediatric
845 B-progenitor acute lymphoblastic leukemia. *Blood* **115**, 5312-5321 (2010).
846 14 Tasian, S. K. *et al.* Potent efficacy of combined PI3K/mTOR and JAK or ABL inhibition in
847 murine xenograft models of Ph-like acute lymphoblastic leukemia. *Blood* **129**, 177-187,
848 doi:10.1182/blood-2016-05-707653 (2017).
849 15 Loh, M. L. *et al.* A phase 1 dosing study of ruxolitinib in children with relapsed or
850 refractory solid tumors, leukemias, or myeloproliferative neoplasms: A Children's

851 Oncology Group phase 1 consortium study (ADVL1011). *Pediatr Blood Cancer* **62**,
852 1717-1724, doi:10.1002/pbc.25575 (2015).
853 16 Maude, S. L. *et al.* Targeting JAK1/2 and mTOR in murine xenograft models of Ph-like
854 acute lymphoblastic leukemia. *Blood* **120**, 3510-3518, doi:10.1182/blood-2012-03-
855 415448 (2012).
856 17 Springuel, L., Renauld, J.-C. & Knoops, L. JAK kinase targeting in hematologic
857 malignancies: a sinuous pathway from identification of genetic alterations towards
858 clinical indications. *Haematologica* **100**, 1240-1253,
859 doi:papers3://publication/doi/10.3324/haematol.2015.132142 (2015).
860 18 Kim, S. K. *et al.* JAK2 is dispensable for maintenance of JAK2 mutant B-cell acute
861 lymphoblastic leukemias. *Genes Dev* **32**, 849-864, doi:10.1101/gad.307504.117 (2018).
862 19 Qin, H. *et al.* Eradication of B-ALL using chimeric antigen receptor-expressing T cells
863 targeting the TSLPR oncoprotein. *Blood* **126**, 629-639, doi:10.1182/blood-2014-11-
864 612903 (2015).
865 20 Brudno, J. N. & Kochenderfer, J. N. Toxicities of chimeric antigen receptor T cells:
866 recognition and management. *Blood* **127**, 3321-3330, doi:10.1182/blood-2016-04-
867 703751 (2016).
868 21 Nikolaev, S. I. *et al.* Frequent cases of RAS-mutated Down syndrome acute
869 lymphoblastic leukaemia lack JAK2 mutations. *Nat Commun* **5**, 4654,
870 doi:10.1038/ncomms5654 (2014).
871 22 Hecker, M., Lambeck, S., Toepfer, S., van Someren, E. & Guthke, R. Gene regulatory
872 network inference: data integration in dynamic models-a review. *Biosystems* **96**, 86-103,
873 doi:10.1016/j.biosystems.2008.12.004 (2009).
874 23 Alsadeq, A. *et al.* Zeta-chain-associated protein kinase-70 (ZAP-70) promotes acute
875 lymphoblastic leukemia (ALL) infiltration into the central nervous system by enhancing
876 chemokine receptor 7 (CCR7) expression. *Blood* **126**, 901 (2015).

877 24 Chai, L. E. *et al.* A review on the computational approaches for gene regulatory network
878 construction. *Comput Biol Med* **48**, 55-65, doi:10.1016/j.compbiomed.2014.02.011
879 (2014).
880 25 Bonneau, R. *et al.* The Inferelator: an algorithm for learning parsimonious regulatory
881 networks from systems-biology data sets de novo. *Genome Biol* **7**, R36, doi:10.1186/gb-
882 2006-7-5-r36 (2006).
883 26 Madar, A., Greenfield, A., Ostrer, H., Vanden-Eijnden, E. & Bonneau, R. The Inferelator
884 2.0: a scalable framework for reconstruction of dynamic regulatory network models. *Conf*
885 *Proc IEEE Eng Med Biol Soc* **2009**, 5448-5451, doi:10.1109/IEMBS.2009.5334018
886 (2009).
887 27 Miraldi, E. R. *et al.* Leveraging chromatin accessibility for transcriptional regulatory
888 network inference in T Helper 17 Cells. *Genome Res* **29**, 449-463,
889 doi:10.1101/gr.238253.118 (2019).
890 28 Castro, D. M., de Veaux, N. R., Miraldi, E. R. & Bonneau, R. Multi-study inference of
891 regulatory networks for more accurate models of gene regulation. *PLoS Comput Biol* **15**,
892 e1006591, doi:10.1371/journal.pcbi.1006591 (2019).
893 29 Arrieta-Ortiz, M. L. *et al.* An experimentally supported model of the Bacillus subtilis
894 global transcriptional regulatory network. *Mol Syst Biol* **11**, 839,
895 doi:10.15252/msb.20156236 (2015).
896 30 Ciofani, M. *et al.* A validated regulatory network for Th17 cell specification. *Cell* **151**,
897 289-303, doi:10.1016/j.cell.2012.09.016 (2012).
898 31 Vagace, J. M. & Gervasini, G. Chemotherapy toxicity in patients with acute leukemia.
899 *INTECH Open Access Publisher* (2011).
900 32 Love, M. I., Huber, W. & Anders, S. Moderated estimation of fold change and dispersion
901 for RNA-seq data with DESeq2. *Genome Biol* **15**, 550, doi:10.1186/s13059-014-0550-8
902 (2014).

903 33 Croker, B. A., Kiu, H. & Nicholson, S. E. SOCS regulation of the JAK/STAT signalling
904 pathway. *Semin Cell Dev Biol* **19**, 414-422, doi:10.1016/j.semcdb.2008.07.010 (2008).
905 34 Yoda, A. *et al.* Functional screening identifies CRLF2 in precursor B-cell acute
906 lymphoblastic leukemia. *Proc Natl Acad Sci U S A* **107**, 252-257,
907 doi:10.1073/pnas.0911726107 (2010).
908 35 McLeay, R. C. & Bailey, T. L. Motif Enrichment Analysis: a unified framework and an
909 evaluation on ChIP data. *BMC Bioinformatics* **11**, 165, doi:10.1186/1471-2105-11-165
910 (2010).
911 36 Greenfield, A., Hafemeister, C. & Bonneau, R. Robust data-driven incorporation of prior
912 knowledge into the inference of dynamic regulatory networks. *Bioinformatics* **29**, 1060-
913 1067, doi:10.1093/bioinformatics/btt099 (2013).
914 37 Schacht, T., Oswald, M., Eils, R., Eichmuller, S. B. & Konig, R. Estimating the activity of
915 transcription factors by the effect on their target genes. *Bioinformatics* **30**, i401-407,
916 doi:10.1093/bioinformatics/btu446 (2014).
917 38 Consolaro, F., Basso, G., Ghaem-Magami, S., Lam, E. W. & Viola, G. FOXM1 is
918 overexpressed in B-acute lymphoblastic leukemia (B-ALL) and its inhibition sensitizes B-
919 ALL cells to chemotherapeutic drugs. *Int J Oncol* **47**, 1230-1240,
920 doi:10.3892/ijo.2015.3139 (2015).
921 39 Zhang, G. *et al.* High ETS2 expression predicts poor prognosis in acute myeloid
922 leukemia patients undergoing allogeneic hematopoietic stem cell transplantation. *Ann*
923 *Hematol* **98**, 519-525, doi:10.1007/s00277-018-3440-4 (2019).
924 40 Fu, L. *et al.* High expression of ETS2 predicts poor prognosis in acute myeloid leukemia
925 and may guide treatment decisions. *J Transl Med* **15**, 159, doi:10.1186/s12967-017-
926 1260-2 (2017).

927 41 Xutao, G. *et al.* BCL11A and MDR1 expressions have prognostic impact in patients with
928 acute myeloid leukemia treated with chemotherapy. *Pharmacogenomics* **19**, 343-348,
929 doi:10.2217/pgs-2017-0157 (2018).
930 42 Wang, F. *et al.* Tight regulation of FOXO1 is essential for maintenance of B-cell
931 precursor acute lymphoblastic leukemia. *Blood* **131**, 2929-2942, doi:10.1182/blood-
932 2017-10-813576 (2018).
933 43 Tomeczkowski, J. *et al.* Absence of G-CSF receptors and absent response to G-CSF in
934 childhood Burkitt's lymphoma and B-ALL cells. *British journal of haematology* **89**, 771-
935 779 (1995).
936 44 Meyer, C. *et al.* Establishment of the B cell precursor acute lymphoblastic leukemia cell
937 line MUTZ-5 carrying a (12:13) translocation. *Leukemia* **15**, 1471-1474 (2001).
938 45 Smith, R. G., Dev, V. G. & Shannon, W. A., Jr. Characterization of a novel human pre-B
939 leukemia cell line. *J Immunol* **126**, 596-602 (1981).
940 46 Yuan, T. *et al.* Regulation of PI3K signaling in T-cell acute lymphoblastic leukemia: a
941 novel PTEN/Ikaros/miR-26b mechanism reveals a critical targetable role for PIK3CD.
942 *Leukemia* **31**, 2355-2364, doi:10.1038/leu.2017.80 (2017).
943 47 Juric, D. *et al.* Differential gene expression patterns and interaction networks in BCR-
944 ABL-positive and -negative adult acute lymphoblastic leukemias. *J Clin Oncol* **25**, 1341-
945 1349, doi:10.1200/JCO.2006.09.3534 (2007).
946 48 Ortiz-Padilla, C. *et al.* Functional characterization of cancer-associated Gab1 mutations.
947 *Oncogene* **32**, 2696-2702, doi:10.1038/onc.2012.271 (2013).
948 49 Poukka, M. *et al.* Acute Lymphoblastic Leukemia With INPP5D-ABL1 Fusion Responds
949 to Imatinib Treatment. *J Pediatr Hematol Oncol* **41**, e481-e483,
950 doi:10.1097/MPH.0000000000001267 (2019).
951 50 Laszlo, G. S. *et al.* High expression of myocyte enhancer factor 2C (MEF2C) is
952 associated with adverse-risk features and poor outcome in pediatric acute myeloid

953 leukemia: a report from the Children's Oncology Group. *J Hematol Oncol* **8**, 115,
954 doi:10.1186/s13045-015-0215-4 (2015).
955 51 Lech-Maranda, E. *et al.* Human leukocyte antigens HLA DRB1 influence clinical
956 outcome of chronic lymphocytic leukemia? *Haematologica* **92**, 710-711,
957 doi:10.3324/haematol.10910 (2007).
958 52 Yao, S., Fan, L. Y. & Lam, E. W. The FOXO3-FOXM1 axis: A key cancer drug target and
959 a modulator of cancer drug resistance. *Semin Cancer Biol* **50**, 77-89,
960 doi:10.1016/j.semcancer.2017.11.018 (2018).
961 53 Liao, G. B. *et al.* Regulation of the master regulator FOXM1 in cancer. *Cell Commun*
962 *Signal* **16**, 57, doi:10.1186/s12964-018-0266-6 (2018).
963 54 Li, X. *et al.* Forkhead box transcription factor 1 expression in gastric cancer: FOXM1 is a
964 poor prognostic factor and mediates resistance to docetaxel. *J Transl Med* **11**, 204,
965 doi:10.1186/1479-5876-11-204 (2013).
966 55 Huynh, K. M. *et al.* FOXM1 expression mediates growth suppression during terminal
967 differentiation of HO-1 human metastatic melanoma cells. *J Cell Physiol* **226**, 194-204,
968 doi:10.1002/jcp.22326 (2011).
969 56 Wang, I. C. *et al.* Foxm1 mediates cross talk between Kras/mitogen-activated protein
970 kinase and canonical Wnt pathways during development of respiratory epithelium. *Mol*
971 *Cell Biol* **32**, 3838-3850, doi:10.1128/MCB.00355-12 (2012).
972 57 Park, Y. Y. *et al.* FOXM1 mediates Dox resistance in breast cancer by enhancing DNA
973 repair. *Carcinogenesis* **33**, 1843-1853, doi:10.1093/carcin/bgs167 (2012).
974 58 Tan, G., Cheng, L., Chen, T., Yu, L. & Tan, Y. Foxm1 mediates LIF/Stat3-dependent
975 self-renewal in mouse embryonic stem cells and is essential for the generation of
976 induced pluripotent stem cells. *PLoS One* **9**, e92304, doi:10.1371/journal.pone.0092304
977 (2014).

978 59 Li, X. *et al.* FOXM1 mediates resistance to docetaxel in gastric cancer via up-regulating
979 Stathmin. *J Cell Mol Med* **18**, 811-823, doi:10.1111/jcmm.12216 (2014).
980 60 Carr, J. R., Park, H. J., Wang, Z., Kiefer, M. M. & Raychaudhuri, P. FoxM1 mediates
981 resistance to herceptin and paclitaxel. *Cancer Res* **70**, 5054-5063, doi:10.1158/0008-
982 5472.CAN-10-0545 (2010).
983 61 Liu, Y. *et al.* FOXM1 overexpression is associated with cisplatin resistance in non-small
984 cell lung cancer and mediates sensitivity to cisplatin in A549 cells via the
985 JNK/mitochondrial pathway. *Neoplasma* **62**, 61-71, doi:10.4149/neo_2015_008 (2015).
986 62 Kong, F. F. *et al.* FOXM1 regulated by ERK pathway mediates TGF-beta1-induced EMT
987 in NSCLC. *Oncol Res* **22**, 29-37, doi:10.3727/096504014X14078436004987 (2014).
988 63 Giangrande, P. H. *et al.* A role for E2F6 in distinguishing G1/S- and G2/M-specific
989 transcription. *Genes Dev* **18**, 2941-2951, doi:10.1101/gad.1239304 (2004).
990 64 Trimarchi, J. M., Fairchild, B., Wen, J. & Lees, J. A. The E2F6 transcription factor is a
991 component of the mammalian Bmi1-containing polycomb complex. *Proc Natl Acad Sci U*
992 *S A* **98**, 1519-1524, doi:10.1073/pnas.041597698 (2001).
993 65 Maity, G. *et al.* The MAZ transcription factor is a downstream target of the oncoprotein
994 Cyr61/CCN1 and promotes pancreatic cancer cell invasion via CRAF-ERK signaling. *J*
995 *Biol Chem* **293**, 4334-4349, doi:10.1074/jbc.RA117.000333 (2018).
996 66 Lee, W. P. *et al.* Akt phosphorylates myc-associated zinc finger protein (MAZ), releases
997 P-MAZ from the p53 promoter, and activates p53 transcription. *Cancer Lett* **375**, 9-19,
998 doi:10.1016/j.canlet.2016.02.023 (2016).
999 67 Tsutsui, H., Sakatsume, O., Itakura, K. & Yokoyama, K. K. Members of the MAZ family:
1000 a novel cDNA clone for MAZ from human pancreatic islet cells. *Biochem Biophys Res*
1001 *Commun* **226**, 801-809, doi:10.1006/bbrc.1996.1432 (1996).

1002 68 Xiao, T., Li, X. & Felsenfeld, G. The Myc-Associated Zinc Finger Protein (MAZ) Works
1003 Both Independently and Together with CTCF to Control Cohesin Positioning and
1004 Genome Organization. *SSRN Electronic Journal*, doi:10.2139/ssrn.3549502 (2020).
1005 69 Wang, W., Xu, S., Yin, M. & Jin, Z. G. Essential roles of Gab1 tyrosine phosphorylation
1006 in growth factor-mediated signaling and angiogenesis. *Int J Cardiol* **181**, 180-184,
1007 doi:10.1016/j.ijcard.2014.10.148 (2015).
1008 70 Yin, J., Xie, X., Ye, Y., Wang, L. & Che, F. BCL11A: a potential diagnostic biomarker and
1009 therapeutic target in human diseases. *Biosci Rep* **39**, doi:10.1042/BSR20190604 (2019).
1010 71 Yu, Y. *et al.* Bcl11a is essential for lymphoid development and negatively regulates p53.
1011 *J Exp Med* **209**, 2467-2483, doi:10.1084/jem.20121846 (2012).
1012 72 Basak, A. & Sankaran, V. G. Regulation of the fetal hemoglobin silencing factor
1013 BCL11A. *Ann N Y Acad Sci* **1368**, 25-30, doi:10.1111/nyas.13024 (2016).
1014 73 Zhang, J. M. *et al.* DPEP1 expression promotes proliferation and survival of leukaemia
1015 cells and correlates with relapse in adults with common B cell acute lymphoblastic
1016 leukaemia. *Br J Haematol*, doi:10.1111/bjh.16505 (2020).
1017 74 Selleri, L. *et al.* The TALE homeodomain protein Pbx2 is not essential for development
1018 and long-term survival. *Mol Cell Biol* **24**, 5324-5331, doi:10.1128/MCB.24.12.5324-
1019 5331.2004 (2004).
1020 75 Schnabel, C. A., Jacobs, Y. & Cleary, M. L. HoxA9-mediated immortalization of myeloid
1021 progenitors requires functional interactions with TALE cofactors Pbx and Meis.
1022 *Oncogene* **19**, 608-616, doi:10.1038/sj.onc.1203371 (2000).
1023 76 Qiu, Y. *et al.* Expression level of Pre B cell leukemia homeobox 2 correlates with poor
1024 prognosis of gastric adenocarcinoma and esophageal squamous cell carcinoma. *Int J*
1025 *Oncol* **36**, 651-663, doi:10.3892/ijo_00000541 (2010).
1026 77 Inamdar, V. V., Reddy, H., Dangelmaier, C., Kostyak, J. C. & Kunapuli, S. P. The protein
1027 tyrosine phosphatase PTPN7 is a negative regulator of ERK activation and thromboxane

1028 generation in platelets. *J Biol Chem* **294**, 12547-12554, doi:10.1074/jbc.RA119.007735
1029 (2019).
1030 78 Seo, H. *et al.* Role of protein tyrosine phosphatase non-receptor type 7 in the regulation
1031 of TNF-alpha production in RAW 264.7 macrophages. *PLoS One* **8**, e78776,
1032 doi:10.1371/journal.pone.0078776 (2013).
1033 79 Turazzi, N. *et al.* Engineered T cells towards TNFRSF13C (BAFFR): a novel strategy to
1034 efficiently target B-cell acute lymphoblastic leukaemia. *Br J Haematol* **182**, 939-943,
1035 doi:10.1111/bjh.14899 (2018).
1036 80 Fazio, G. *et al.* TNFRSF13C (BAFFR) positive blasts persist after early treatment and at
1037 relapse in childhood B-cell precursor acute lymphoblastic leukaemia. *Br J Haematol* **182**,
1038 434-436, doi:10.1111/bjh.14794 (2018).
1039 81 McWilliams, E. M. *et al.* Anti-BAFF-R antibody VAY-736 demonstrates promising
1040 preclinical activity in CLL and enhances effectiveness of ibrutinib. *Blood Adv* **3**, 447-460,
1041 doi:10.1182/bloodadvances.2018025684 (2019).
1042 82 Ke, J. *et al.* The role of MAPKs in B cell receptor-induced down-regulation of Egr-1 in
1043 immature B lymphoma cells. *J Biol Chem* **281**, 39806-39818,
1044 doi:10.1074/jbc.M604671200 (2006).
1045 83 Wasylyk, B., Hagman, J. & Gutierrez-Hartmann, A. Ets transcription factors: nuclear
1046 effectors of the Ras-MAP-kinase signaling pathway. *Trends Biochem Sci* **23**, 213-216,
1047 doi:10.1016/s0968-0004(98)01211-0 (1998).
1048 84 Daud, S. S. *et al.* Identification of the Wnt Signalling Protein, TCF7L2 As a Significantly
1049 Overexpressed Transcription Factor in AML. *Blood* **120**, 1281-1281,
1050 doi:10.1182/blood.V120.21.1281.1281 (2012).
1051 85 Hornsveld, M., Dansen, T. B., Derksen, P. W. & Burgering, B. M. T. Re-evaluating the
1052 role of FOXOs in cancer. *Semin Cancer Biol* **50**, 90-100,
1053 doi:10.1016/j.semcancer.2017.11.017 (2018).

1054 86 Dinkel, A. *et al.* The transcription factor early growth response 1 (Egr-1) advances
1055 differentiation of pre-B and immature B cells. *J Exp Med* **188**, 2215-2224,
1056 doi:10.1084/jem.188.12.2215 (1998).
1057 87 Buenrostro, J. D., Giresi, P. G., Zaba, L. C., Chang, H. Y. & Greenleaf, W. J.
1058 Transposition of native chromatin for fast and sensitive epigenomic profiling of open
1059 chromatin, DNA-binding proteins and nucleosome position. *Nat Methods* **10**, 1213-1218,
1060 doi:10.1038/nmeth.2688 (2013).
1061 88 Kim, D. *et al.* TopHat2: accurate alignment of transcriptomes in the presence of
1062 insertions, deletions and gene fusions. *Genome Biol* **14**, R36, doi:10.1186/gb-2013-14-4-
1063 r36 (2013).
1064 89 Anders, S., Pyl, P. T. & Huber, W. HTSeq--a Python framework to work with high-
1065 throughput sequencing data. *Bioinformatics* **31**, 166-169,
1066 doi:10.1093/bioinformatics/btu638 (2015).
1067 90 Ramirez, F. *et al.* deepTools2: a next generation web server for deep-sequencing data
1068 analysis. *Nucleic Acids Res* **44**, W160-165, doi:10.1093/nar/gkw257 (2016).
1069 91 Langmead, B. & Salzberg, S. L. Fast gapped-read alignment with Bowtie 2. *Nat Methods*
1070 **9**, 357-359, doi:10.1038/nmeth.1923 (2012).
1071 92 Giannopoulou, E. G. & Elemento, O. An integrated ChIP-seq analysis platform with
1072 customizable workflows. *BMC Bioinformatics* **12**, 277, doi:10.1186/1471-2105-12-277
1073 (2011).
1074 93 Dobin, A. *et al.* STAR: ultrafast universal RNA-seq aligner. *Bioinformatics* **29**, 15-21,
1075 doi:10.1093/bioinformatics/bts635 (2013).
1076 94 Weirauch, M. T. *et al.* Determination and inference of eukaryotic transcription factor
1077 sequence specificity. *Cell* **158**, 1431-1443, doi:10.1016/j.cell.2014.08.009 (2014).
1078 95 Grant, C. E., Bailey, T. L. & Noble, W. S. FIMO: scanning for occurrences of a given
1079 motif. *Bioinformatics* **27**, 1017-1018, doi:10.1093/bioinformatics/btr064 (2011).

Figure 1

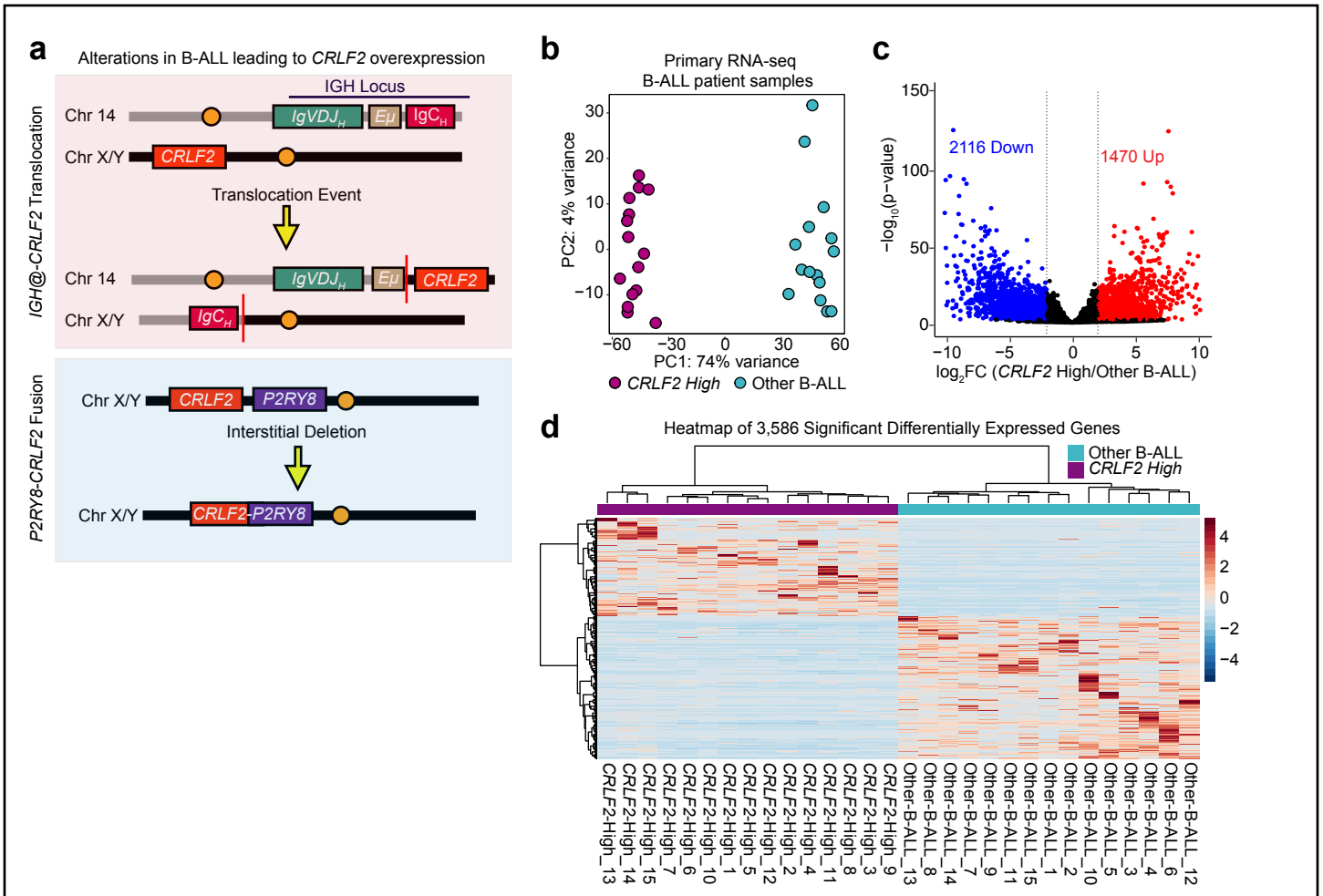
a
Alterations in B-ALL leading to CRLF2 overexpression
IGH@-CRLF2 Translocation
IGH Locus
Chr 14
IgVDJH
Eμ
IgCH
Chr X/Y
CRLF2
Translocation Event
Chr 14
IgVDJH
Eμ
CRLF2
Chr X/Y
IgCH
P2RY8-CRLF2 Fusion
Chr X/Y
CRLF2
P2RY8
Interstitial Deletion
Chr X/Y
CRLF2-P2RY8
b
Primary RNA-seq
B-ALL patient samples
PC2: 4% variance
PC1: 74% variance
CRLF2 High
Other B-ALL
c
2116 Down
1470 Up
−log10(p−value)
log2FC (CRLF2 High/Other B-ALL)
d
Heatmap of 3,586 Significant Differentially Expressed Genes
Other B-ALL
CRLF2 High
CRLF2-High_13
CRLF2-High_14
CRLF2-High_15
CRLF2-High_7
CRLF2-High_6
CRLF2-High_10
CRLF2-High_1
CRLF2-High_5
CRLF2-High_12
CRLF2-High_2
CRLF2-High_4
CRLF2-High_11
CRLF2-High_8
CRLF2-High_3
CRLF2-High_9
Other-B-ALL_13
Other-B-ALL_8
Other-B-ALL_14
Other-B-ALL_7
Other-B-ALL_9
Other-B-ALL_11
Other-B-ALL_15
Other-B-ALL_1
Other-B-ALL_2
Other-B-ALL_10
Other-B-ALL_5
Other-B-ALL_3
Other-B-ALL_4
Other-B-ALL_6
Other-B-ALL_12

Figure 1: Genome-wide transcriptional changes in CRLF2-overexpressing primary patient samples. (a) Schematic of chromosomal alterations, IGH-CRLF2 (top) and P2RY2-CRLF2 (bottom) leading to CRLF2 overexpression. (b) PCA analysis of 15 CRLF2-High (purple, n=15) and 15 Other B-ALL (teal, n=15) patient RNA-seq samples. (c) Volcano plot of the differentially expressed genes (DESeq2: FDR=1%, |log2 fold change| >2) between CRLF2-High and other B-ALL patients. Red and blue points correspond to up and down-regulated genes (n=1470 and 2116, respectively) in CRLF2-High samples. (d) Expression heatmap of 3,586 differentially expressed genes across patient samples.

Figure 2

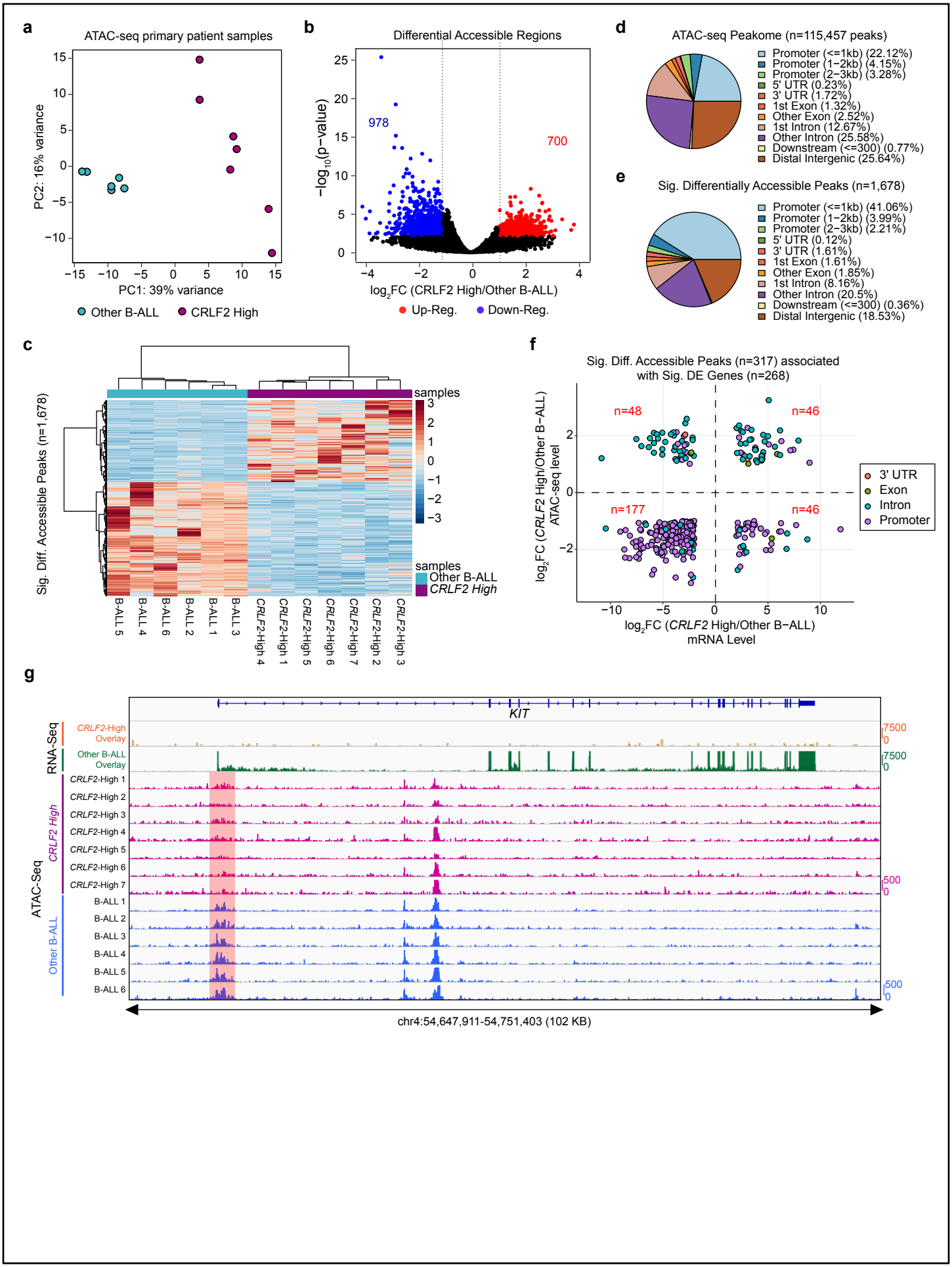
a
ATAC-seq primary patient samples
PC2: 16% variance
PC1: 39% variance
Other B-ALL
CRLF2 High
b
Differential Accessible Regions
−log10(p−value)
978
700
log2FC (CRLF2 High/Other B-ALL)
Up-Reg.
Down-Reg.
d
ATAC-seq Peakome (n=115,457 peaks)
Promoter (<=1kb) (22.12%)
Promoter (1−2kb) (4.15%)
Promoter (2−3kb) (3.28%)
5' UTR (0.23%)
3' UTR (1.72%)
1st Exon (1.32%)
Other Exon (2.52%)
1st Intron (12.67%)
Other Intron (25.58%)
Downstream (<=300) (0.77%)
Distal Intergenic (25.64%)
e
Sig. Differentially Accessible Peaks (n=1,678)
Promoter (<=1kb) (41.06%)
Promoter (1−2kb) (3.99%)
Promoter (2−3kb) (2.21%)
5' UTR (0.12%)
3' UTR (1.61%)
1st Exon (1.61%)
Other Exon (1.85%)
1st Intron (8.16%)
Other Intron (20.5%)
Downstream (<=300) (0.36%)
Distal Intergenic (18.53%)
c
Sig. Diff. Accessible Peaks (n=1,678)
samples
Other B-ALL
CRLF2 High
B-ALL 5
B-ALL 4
B-ALL 6
B-ALL 2
B-ALL 1
B-ALL 3
CRLF2-High 4
CRLF2-High 1
CRLF2-High 5
CRLF2-High 6
CRLF2-High 7
CRLF2-High 2
CRLF2-High 3
f
Sig. Diff. Accessible Peaks (n=317) associated with Sig. DE Genes (n=268)
n=48
n=46
n=177
n=46
log2FC (CRLF2 High/Other B−ALL) ATAC-seq level
log2FC (CRLF2 High/Other B−ALL) mRNA Level
3' UTR
Exon
Intron
Promoter
g
KIT
RNA-Seq
CRLF2-High Overlay
Other B-ALL Overlay
ATAC-Seq
CRLF2 High
Other B-ALL
CRLF2-High 1
CRLF2-High 2
CRLF2-High 3
CRLF2-High 4
CRLF2-High 5
CRLF2-High 6
CRLF2-High 7
B-ALL 1
B-ALL 2
B-ALL 3
B-ALL 4
B-ALL 5
B-ALL 6
7500
0
500
chr4:54,647,911-54,751,403 (102 KB)

Figure 2: CRLF2-overexpression leads to promoter-enriched ATAC-seq changes in primary patient samples. (a) PCA analysis of 7 CRLF2-High (purple) and 6 Other B-ALL (teal) ATAC-seq samples. (b) Volcano plot of the differential accessible peaks (DESeq2: FDR=1%, |log2 fold change| >1) between CRLF2-High and other B-ALL patients. Red and blue points correspond to more accessible and less accessible ATAC-seq peaks, respectively (n=700 and 978,) in CRLF2-High samples. (c) Heatmap of 700 more accessible (purple bar) and 978 less accessible ATAC-seq peaks in CRLF2-High patients. (d) ChIPseeker genomic annotation of all ATAC-seq peaks or Peakome (n=115,457) across all patient samples. (e) ChIPseeker genomic annotation of significantly differential ATAC-seq peaks (n=1678). (f) Differentially ATAC-seq peaks (n=317), excluding peaks in distal intergenic regions, linked to differentially expressed genes (n=268) and the log2 fold change of gene expression (x-axis) plotted against the log2 fold change of ATAC-seq reads (y-axis). Linked genes are colored according to genomic annotation. (g) IGV screenshot of ATAC-seq tracks for individual samples at down-regulated KIT gene, RNA-seq tracks for CRLF2-High (orange) and other B-ALL (green) samples are overlayed. The highlighted region indicates a region of decreasing accessibility in CRLF2-High samples.

Figure 3

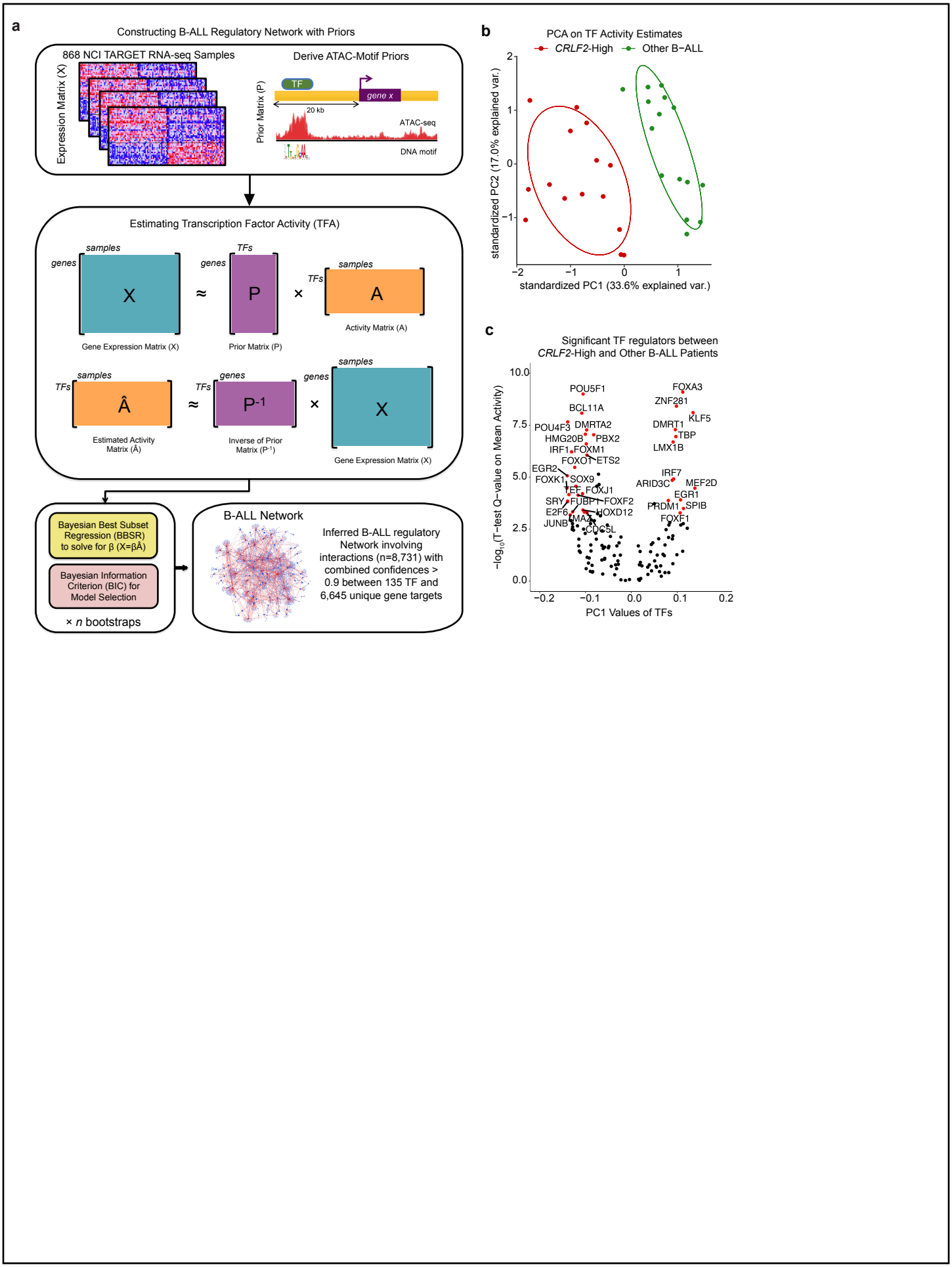
a
Constructing B-ALL Regulatory Network with Priors
868 NCI TARGET RNA-seq Samples
Expression Matrix (X)
Derive ATAC-Motif Priors
Prior Matrix (P)
TF
gene x
20 kb
ATAC-seq
DNA motif
Estimating Transcription Factor Activity (TFA)
samples
genes
X
Gene Expression Matrix (X)
≈
TFs
P
Prior Matrix (P)
×
A
Activity Matrix (A)
Â
Estimated Activity Matrix (Â)
P-1
Inverse of Prior Matrix (P-1)
Bayesian Best Subset Regression (BBSR) to solve for β (X=βÂ)
Bayesian Information Criterion (BIC) for Model Selection
× n bootstraps
B-ALL Network
Inferred B-ALL regulatory Network involving interactions (n=8,731) with combined confidences > 0.9 between 135 TF and 6,645 unique gene targets
b
PCA on TF Activity Estimates
CRLF2-High
Other B−ALL
standardized PC2 (17.0% explained var.)
standardized PC1 (33.6% explained var.)
c
Significant TF regulators between CRLF2-High and Other B-ALL Patients
−log10(T−test Q−value on Mean Activity)
PC1 Values of TFs
POU5F1
BCL11A
POU4F3
DMRTA2
HMG20B
PBX2
IRF1
FOXM1
FOXO1
ETS2
EGR2
FOXK1
SOX9
ETS1
FOXJ1
SRY
FUBP1
FOXF2
E2F6
FOXD12
JUNB
MAX
CDC5L
FOXA3
ZNF281
KLF5
DMRT1
TBP
LMX1B
IRF7
ARID3C
MEF2D
EGR1
PRDM1
SPIB
FOXF1

Figure 3: B-ALL network inference identifies significant TFs in the CRLF2-High patient cohort. (a) Workflow for construction of B-ALL regulatory network using Bayesian Best Subset Regression with the Inferelator algorithm. Inferelator resulted in a B-ALL regulatory network involving interactions (n=8,731) with combined confidences > 0.9 between 135 TF and 6,645 unique gene targets. (b) PCA of 30 primary patient samples computed according to estimated TF activity values of 135 TFs. (c) Volcano plot of the significant differential TFs (FDR=0.1%, |PC1 value| >0.075) between CRLF2-High and other B-ALL patients. Red points indicate highly variable TFs between two conditions with significant differential mean activity (t-test; q-value<0.001).

Figure 4

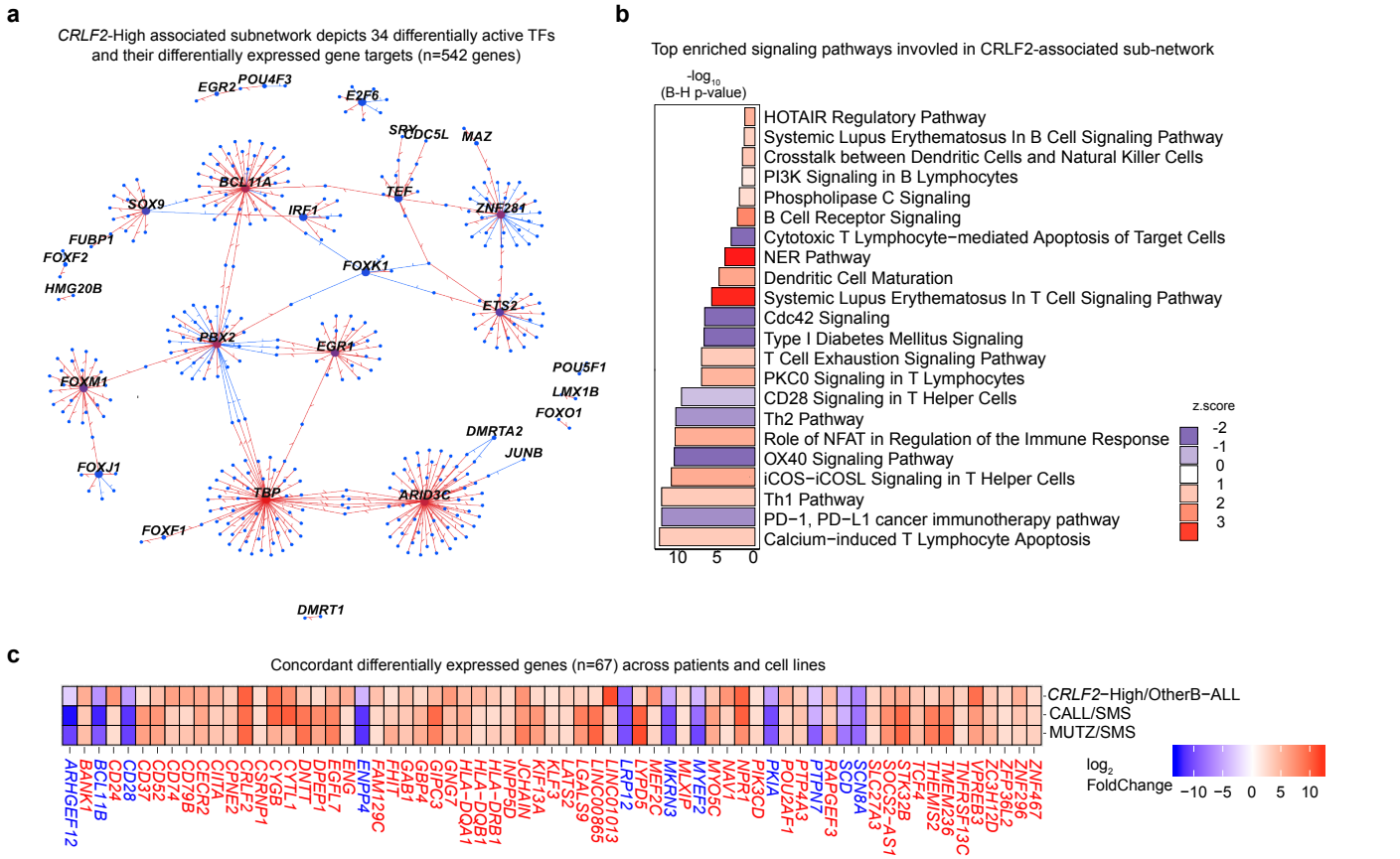
a
CRLF2-High associated subnetwork depicts 34 differentially active TFs and their differentially expressed gene targets (n=542 genes)
EGR2
POU4F3
E2F6
SRY
CDC5L
MAZ
BCL11A
SOX9
IRF1
TEF
ZNF281
FUBP1
FOXF2
HMG20B
FOXK1
ETS2
PBX2
EGR1
POU5F1
FOXM1
LMX1B
FOXO1
DMRTA2
JUNB
FOXJ1
TBP
ARID3C
FOXF1
DMRT1
b
Top enriched signaling pathways invovled in CRLF2-associated sub-network
-log10 (B-H p-value)
HOTAIR Regulatory Pathway
Systemic Lupus Erythematosus In B Cell Signaling Pathway
Crosstalk between Dendritic Cells and Natural Killer Cells
PI3K Signaling in B Lymphocytes
Phospholipase C Signaling
B Cell Receptor Signaling
Cytotoxic T Lymphocyte−mediated Apoptosis of Target Cells
NER Pathway
Dendritic Cell Maturation
Systemic Lupus Erythematosus In T Cell Signaling Pathway
Cdc42 Signaling
Type I Diabetes Mellitus Signaling
T Cell Exhaustion Signaling Pathway
PKC0 Signaling in T Lymphocytes
CD28 Signaling in T Helper Cells
Th2 Pathway
Role of NFAT in Regulation of the Immune Response
OX40 Signaling Pathway
iCOS−iCOSL Signaling in T Helper Cells
Th1 Pathway
PD−1, PD−L1 cancer immunotherapy pathway
Calcium−induced T Lymphocyte Apoptosis
10 5 0
z.score
-2
-1
0
1
2
3
c
Concordant differentially expressed genes (n=67) across patients and cell lines
CRLF2−High/OtherB−ALL
CALL/SMS
MUTZ/SMS
ARHGEF12 BANK1 BCL11B CD24 CD28 CD37 CD52 CD74 CD79B CECR2 CIITA CPNE2 CRLF2 CSRNP1 CYGB CYTL1 DNTT DPEP1 EGFL7 ENG ENPP4 FAM129C FHIT GAB1 GBP4 GJFC3 GNG7 HLA-DQA1 HLA-DQB1 HLA-DRB1 INPP5D JCHAIN KIF13A KLF3 LATS2 LGALS9 LINC00865 LINC01013 LRP12 LYPD5 MEF2C MKRN3 MLXIP MYEF2 MYO5C NAV1 NPR1 PIK3CD PKIA POU2AF1 PTPN4 PTPN7 RAPGEF3 SCN8A SCD SLC27A3 SOCS2-AS1 STK32B TCF4 THEMIS2 TMEM236 TNFRSF13C VPREB3 ZC3H12D ZFP36L2 ZNF296 ZNF467
log2 FoldChange
−10 −5 0 5 10

Figure 4: Significant TFs predicted to regulate conserved differentially expressed gene targets across patients and cell lines. (a) Filtered B-ALL network involving regulatory interactions between significant TFs (n=34) and their differentially expressed gene targets (n=542). TFs are the source nodes labeled in black and the gene targets are the blue target nodes. The size of the source nodes reflects the number of targets each TF has. TF activation and repression of a gene are represented by red and blue edges, respectively. (b) Significant pathways (–log10(B-H p-value > 1.3 & |z-score| > 1) identified from analysis of differential gene targets in the CRLF2 specific sub-network are shown at the top of the figure, ranked by the –log10(Benjamini-Hochberg p-value). Z-score in the bar plot indicates sign of the pathway with red and blue representing up- and down-regulation of the pathway. (c) Log2 fold changes of all the convergent differentially expressed gene targets in CRLF2-High vs other B-ALL patients and cell lines (CALL vs SMS, MUTZ vs SMS).

Figure 5

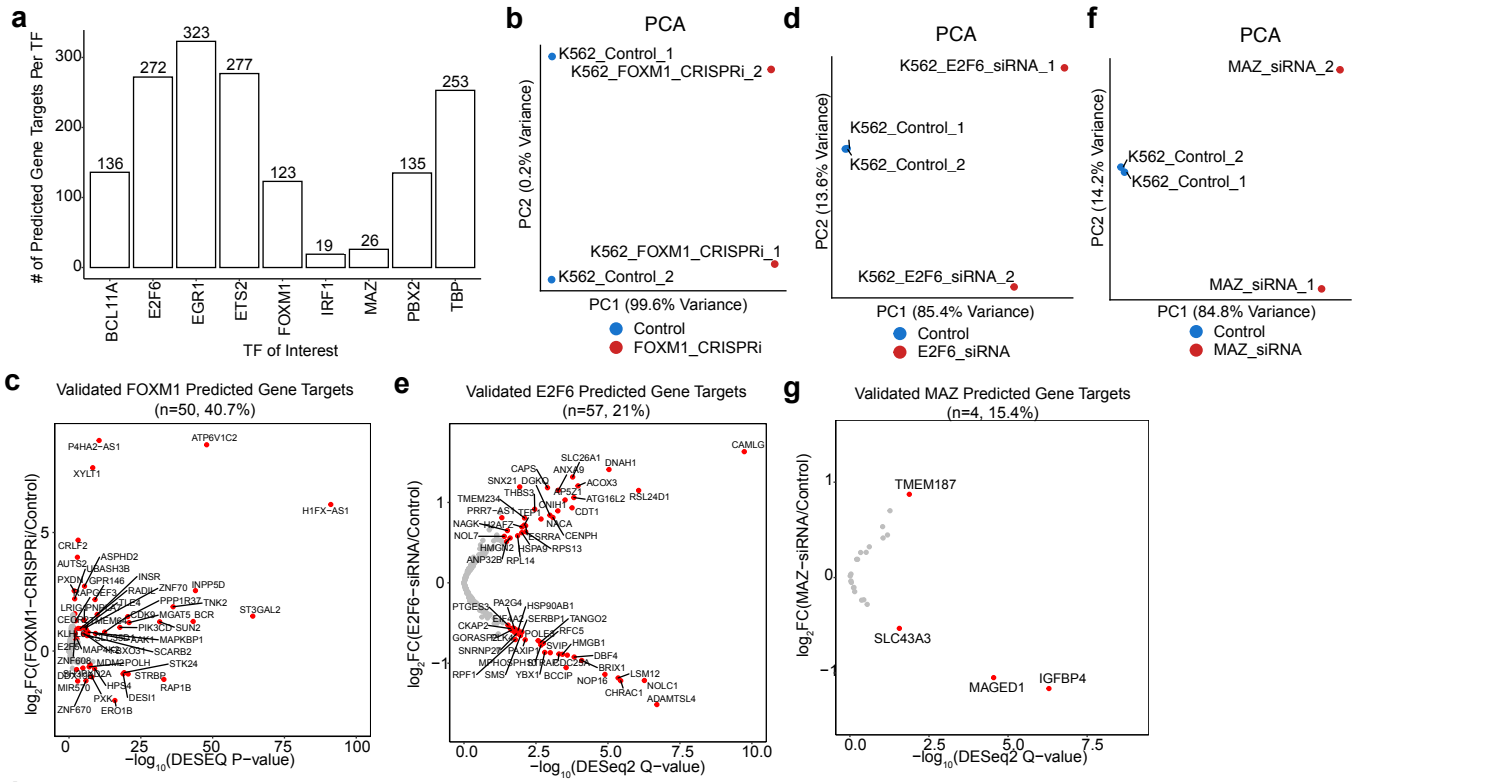

h

TF of Interest	Experiment	Predicted Gene Targets per TF	# Optimal IDR ChIP-seq Peaks	# of Genes associated with atleast one Peak	# of Validated Predicted Gene Targets with TF ChIP-seq peak
IRF1	ChIP-seq (K562)	19	1,483	1,289	5
BCL11A	ChIP-seq (GM12878)	136	20,663	8,452	56
TBP	ChIP-seq (K562)	253	22,063	11,411	121
PBX2	ChIP-seq (K562)	135	36,585	12,961	77
EGR1	ChIP-seq (K562)	323	30,044	13,161	223
ETS2	ChIP-seq (K562)	277	1,705	1,216	17

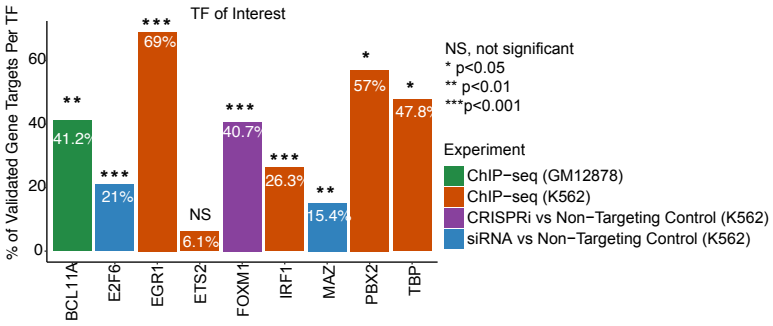

Figure 5: Validating inferred gene targets of TFs significantly altered by *CRLF2* overexpression. (a) Bar plot representing the number of predicted gene targets for 9 TFs, for which public data was available for validation. Exact numbers are represented at the top of the bar. (b) PCA analysis of 4 CRISPRi targeting FOXM1 (red) and non-targeting control (blue) RNA-seq samples. (c) Volcano plot of the FOXM1 predicted gene targets, those that are differentially expressed genes (FDR=5%, |log2 fold change| >0.5) between FOXM1 CRISPRi and non-targeting control samples are highlighted in red and labeled. (d) PCA analysis of 4 CRISPRi targeting E2F6 (red) and non-targeting control (blue) RNA-seq samples. (e) Volcano plot of the E2F6 predicted gene targets, those that are differentially expressed genes (FDR=5%, |log2 fold change| >0.5) between E2F6 CRISPRi and non-targeting control samples are highlighted in red and labeled. (f) PCA analysis of 4 CRISPRi targeting MAZ (red) and non-targeting control (blue) RNA-seq samples. (g) Volcano plot of the MAZ predicted gene targets, those that are differentially expressed genes (FDR=5%, |log2 fold change| >0.5) between MAZ CRISPRi and non-targeting control samples are highlighted in red and labeled. (h) Table representing the ENCODE ChIP-seq experiments for 6 TFs, including the TF of interest, the experiment, number of predicted gene targets from the B-ALL network, number of optimal IDR ChIP-seq peaks, number of annotated genes with at least one ChIP-seq peak, and finally the number of validated gene targets for each TF of interest. (i) Barplot representing the percentage of validated gene targets for each of the 9 TFs of interest. The percentage of validated inferred gene targets for each TF is labeled in white at the top of the bar. P-values obtained from hyper-geometric test are annotated as follows: NS, not significant; *, $p < 0.05$, $p<0.01$, $p<0.001$. Color of the bar represents the experiment.

Figure 6

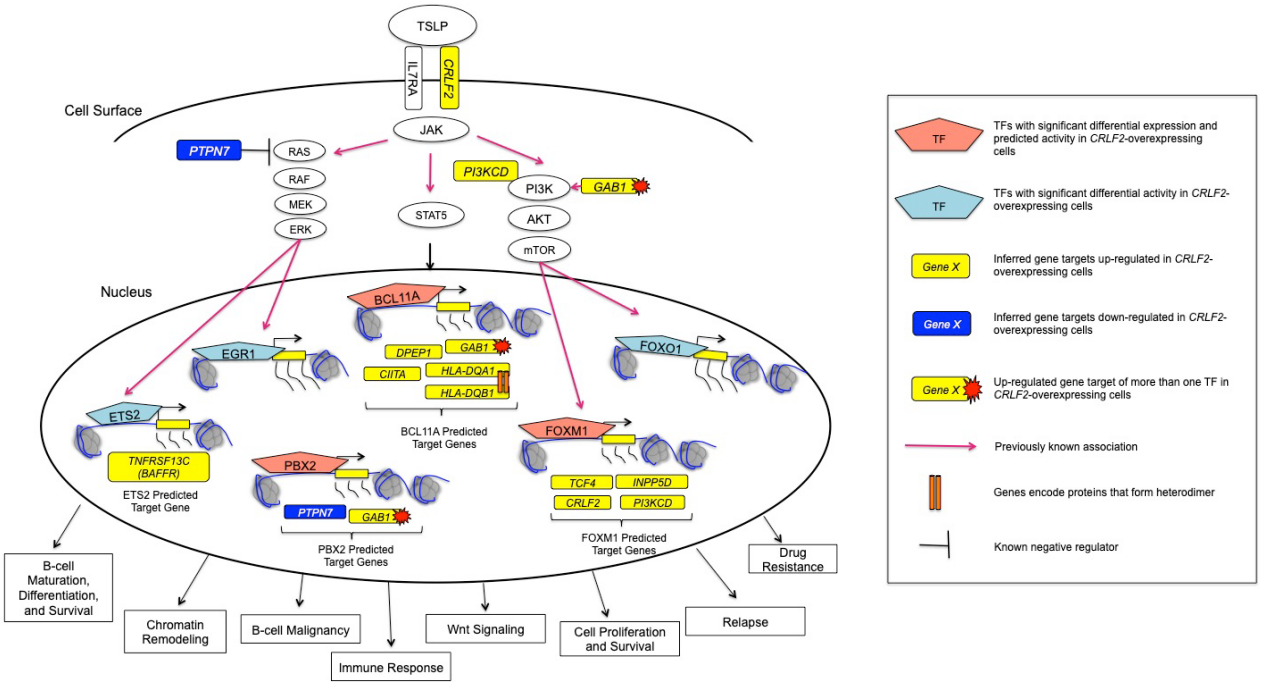
a
Inferred Transcriptional Regulatory Interactions Downstream of CRLF2-mediated Signaling in B-ALL
TSLP
IL7RA
CRLF2
Cell Surface
JAK
PTPN7
RAS
RAF
MEK
ERK
PI3KCD
PI3K
GAB1
STAT5
AKT
mTOR
Nucleus
BCL11A
DPEP1
GAB1
CIITA
HLA-DQA1
HLA-DQB1
BCL11A Predicted Target Genes
EGR1
FOXO1
ETS2
TNFRSF13C (BAFFR)
ETS2 Predicted Target Gene
PBX2
PTPN7
GAB1
PBX2 Predicted Target Genes
FOXM1
TCF4
INPP5D
CRLF2
PI3KCD
FOXM1 Predicted Target Genes
B-cell Maturation, Differentiation, and Survival
Chromatin Remodeling
B-cell Malignancy
Immune Response
Wnt Signaling
Cell Proliferation and Survival
Relapse
Drug Resistance
TF
TFs with significant differential expression and predicted activity in CRLF2-overexpressing cells
TF
TFs with significant differential activity in CRLF2-overexpressing cells
Gene X
Inferred gene targets up-regulated in CRLF2-overexpressing cells
Gene X
Inferred gene targets down-regulated in CRLF2-overexpressing cells
Gene X
Up-regulated gene target of more than one TF in CRLF2-overexpressing cells
Previously known association
Genes encode proteins that form heterodimer
Known negative regulator

Figure 6: Proposed Model. (a) Inferred transcriptional regulatory interactions downstream of CRLF2-mediated signaling in B-ALL.